Improvement and Further Development in CESM/CAM5: Gas-Phase Chemistry and Inorganic Aerosol Treatments

Jian He[1] and Yang Zhang[1,*]

[1]Air Quality Forecasting Laboratory, Department of Marine, Earth, and Atmospheric Sciences, North Carolina State University, Raleigh, NC, 27695, USA

Abstract: Gas-phase chemistry and subsequent gas-to-particle conversion processes such as new particle formation (J), condensation, and thermodynamic partitioning have large impacts on air quality, climate, and public health through influencing the amounts and distributions of gaseous precursors and secondary aerosols. Their roles in global air quality and climate are examined in this work using the Community Earth System Model version 1.0.5 (CESM1.0.5) with the Community Atmosphere Model version 5.1 (CAM5.1) (referred to as CESM1.0.5/CAM5.1). CAM5.1 includes a simple chemistry that is coupled with a 7-mode prognostic Modal Aerosol Model (MAM7). MAM7 includes classical homogenous nucleation (binary and ternary) and activation nucleation (empirical first-order power law) parameterizations, and a highly-simplified inorganic aerosol thermodynamics treatment that only simulates particulate-phase sulfate and ammonium. In this work, a new gas-phase chemistry mechanism based on the 2005 Carbon Bond Mechanism for Global Extension (CB05_GE) and several advanced inorganic aerosol treatments for condensation of volatile species, ion-mediated nucleation (IMN), and explicit inorganic aerosol thermodynamics for sulfate, ammonium, nitrate, sodium, and chloride have been incorporated into CESM/CAM5.1-MAM7. Comparing to the simple gas-phase chemistry, CB05_GE can predict many more gaseous species, and thus could improve model performance for $PM_{2.5}$, PM_{10}, PM components, and some PM gaseous precursors such as SO_2 and NH_3 in several regions, as well as aerosol optical depth (AOD) and cloud properties (e.g., cloud fraction

* Email: yang_zhang@ncsu.edu, Phone: (919)-515-9688

(CF), cloud droplet number concentration (CDNC), and shortwave cloud forcing (SWCF)) on globe. The modified condensation and aqueous-phase chemistry could further improve the predictions of additional variables such as HNO_3, NO_2, and O_3 in some regions, and new particle formation rate (J) and AOD over globe. IMN can improve the predictions of secondary $PM_{2.5}$ components, $PM_{2.5}$, and PM_{10} over Europe, as well as AOD and CDNC over globe. The explicit inorganic aerosol thermodynamics using ISORROPIA II improves the predictions of all major $PM_{2.5}$ components and their gaseous precursors in some regions, as well as downwelling shortwave radiation, SWCF, and cloud condensation nuclei at a supersaturation of 0.5% over globe. For simulations of 2001-2005 with all the modified and new treatments, the improved model predicts that on a global average, SWCF increases by 2.7 W m^{-2}, reducing NMBs of SWCF from -5.4% to 1.2%. Uncertainties in emissions can explain largely the inaccurate predictions of precursor gases (e.g., SO_2, NH_3, and NO) and primary aerosols (e.g., black carbon and primary organic matter). Additional factors leading to discrepancies between model predictions and observations include assumptions associated with equilibrium partitioning for fine particles assumed in ISORROPIA II, irreversible gas/particle mass transfer treatment for coarse particles, uncertainties in model treatments such as dust emissions, secondary organic aerosol formation, multiple-phase chemistry, cloud microphysics, aerosol-cloud interaction, dry and wet deposition, and model parameters (e.g., accommodation coefficients and prefactors of the nucleation power law), as well as uncertainties in model configuration such as the use of a coarse grid resolution.

Keywords: CESM/CAM5.1, CB05_GE, New particle formation, Aerosol thermodynamics, Ion-mediated nucleation, ISORROPIA II, Earth system modeling

1. Introduction

Atmospheric gases and aerosols play important roles in atmosphere and Earth system due to their ability to alter the Earth's radiation balance. Atmospheric chemistry determines the formation of ozone (O_3) and fine particular matter ($PM_{2.5}$) through affecting the distribution of oxidants and their gaseous precursors. Different chemical reactions and kinetic parameters can lead to differences in the predictions of gases, secondary aerosols, new particle formation rate (J), as well as climatic variables such as cloud condensation nuclei (CCN), cloud droplet number concentration (CDNC), and radiative forcing (Faraji et al., 2008; Zhang et al., 2012a). Meanwhile, climate change can strongly influence atmospheric chemistry and air quality.

Aerosol can influence the Earth's radiative balance by directly scattering and absorbing radiation and indirectly affecting cloud properties through acting as CCN and ice nuclei (IN). Therefore, it is important to accurately simulate aerosol size distribution, chemical composition, and properties, which can determine the magnitude of aerosol radiative forcing (Koloutsou-Vakakis et al., 1998). Aerosol and its influence on climate have been included in many global climate models (GCMs) such as the Community Climate System Model (CCSM) (Collins et al., 2006), the 5th generation of global climate model modified from European Centre for Medium-Range Weather Forecasts in Hamburg (ECHAM5) (Stier et al., 2005), and Earth system models such as the Community Earth System Model (CESM) (Ghan et al., 2012; Liu et al., 2012), the Integrated Global System Model (IGSM) (Dutkiewicz et al., 2005; Sokolov et al., 2005), and the Earth System Model (ESM) (Dunne et al., 2012). However, due to the complexity of aerosol microphysical processes and their interactions with cloud processes, it remains a challenge to accurately represent those properties and processes in GCMs.

Inorganic aerosols comprise 25-50% of fine aerosol mass (Heintzenberg, 1989), which mainly includes sulfate (SO_4^{2-}), ammonium (NH_4^+), nitrate (NO_3^-), chloride (Cl^-), and sodium (Na^+). Major gas-to-particle conversion processes of inorganic aerosols include condensation, nucleation, and thermodynamics. An important factor that determines the condensation of gases is the mass accommodation coefficient (α), which can be measured through laboratory experiments. The measured α values, however, are subject to large uncertainty and may vary in several orders of magnitudes under different laboratory conditions. To simulate aerosol condensational growth, a constant value of α is therefore often assumed in GCMs, which is a source of uncertainty in model predictions.

Homogeneous nucleation of H_2SO_4 vapor produces new particles that can grow to form CCN. Different nucleation parameterizations are used in GCMs or global aerosol models. For example, Sihto et al. (2006) derived empirical power laws with the first- or second-order dependencies of new particle formation rates (J) on H_2SO_4 vapor concentration from observations based on cluster-activation or barrierless kinetic mechanisms, which have been used in the Community Atmosphere Model (CAM) (Wang and Penner, 2009), the Global-through-Urban Weather Research and Forecasting model with Chemistry (GU-WRF/Chem) (Zhang et al., 2012b), and Global Model of Aerosol Processes (GLOMAP) (Spracklen et al., 2006). An ion-mediated nucleation (IMN) model was developed to calculate J based on ambient atmospheric conditions, H_2SO_4 vapor concentrations, ionization rate, and surface area of preexisting particles. It has been used in GEOS-Chem (Yu et al., 2008), CAM (Yu et al., 2012), and GU_WRF/Chem (Zhang et al., 2012b). Different nucleation parameterizations lead to significant differences in J predictions by regional and global models (Zhang et al., 2010) and CCN/CDNC (Zhang et al.,

94 2012b; Yu et al., 2012). Limited observations make it difficult to validate predicted J values and
95 appropriateness of various parameterizations.
96 A number of thermodynamic aerosol modules have been developed to understand physical and
97 chemical properties of inorganic aerosols. For example, EQUISOLV II (Jacobson, 1999) has
98 been used in a one-way nested (from global to local scales) gas, aerosol, transport, radiation,
99 general circulation, mesoscale, and ocean model (GATOR-GCMOM) (Jacobson, 2010).
100 EQUISOLV II uses analytical equilibrium iteration and mass flux iteration to solve equilibrium
101 problems (Jacobson, 1999), which requires relatively large computational cost. SCAPE2 is used
102 in the California Institute of Technology (CIT) model (Meng et al., 1998). ISORROPIA (Nenes
103 et al., 1998) has been used in several global models such as GEOS-Chem (Bey et al., 2001), the
104 GISS Caltech (Liao et al., 2003), and the GU-WRF/Chem (Zhang et al., 2012b) and regional
105 models such as the Community Multiscale Air Quality model (CMAQ) (Byun and Schere, 2006)
106 and the Comprehensive Air Quality Model with Extensions (CAMx) (ENVIRON, 2010). An
107 updated version, ISORROPIA II (Fountoukis and Nenes, 2007), has also been implemented in
108 recent versions of CMAQ (e.g., CMAQ v4.7-Dust (Wang et al., 2012) and CMAQ v5.0 (Appel et
109 al., 2013)), GEOS-Chem (Fountoukis and Nenes, 2007), and ECHAM5 with MESSy
110 Atmospheric Chemistry and Global Modal-aerosol eXtension (EMAC/GMXe) (Metzger et al.,
111 2011). The Multicomponent Equilibrium Solver for Aerosols (MESA) (Zaveri et al., 2005) has
112 been used in the mesoscale WRF/Chem (Fast et al., 2006). These modules assume that particles
113 simulated in a given particle size range have the same composition (i.e., internal mixture).
114 Different aerosol thermodynamic models can lead to different aerosol predictions (Nenes et al.,
115 1998; Zhang et al., 2000; Zaveri et al., 2005). Zhang et al (2000) reported average absolute
116 differences of 7.7% - 12.3% in total PM predictions between different thermodynamic modules

under 400 test conditions but the differences could be as large as 68% under some cases (e.g., high nitrate/chloride and low/medium relative humidity (RH)). Fountoukis and Nenes (2007) found the largest discrepancies between ISORROPIA II and SCAPE2 in water concentration predictions exist under low RH conditions (RH < 60%), primarily from differences in the treatment of water uptake and solid state composition. The 3-D atmospheric models with these modules include explicit thermodynamic treatments for sulfate, ammonium, nitrate, sodium, and chloride. The equilibrium assumption, however, is not valid under some conditions (e.g., coarse particles and cooler conditions) (Meng and Seinfeld, 1996). Kinetic approaches are therefore needed to treat gas/particle mass transfer under such conditions. Kinetic approaches, on the other hand, are computationally expensive (Zhang et al., 2004; Hu et al., 2008) and have only been implemented in a few 3-D models (e.g., Meng and Seinfeld, 1996; Jacobson, 2005; Zhang and Wexler, 2006; Zaveri et al., 2008). A hybrid approach that assumes equilibrium for fine particles and solves gas/particle mass transfer for coarse particles has been thus developed, which provides the best compromise between numerical accuracy and computational efficiency (Capaldo et al., 2000; Kelly et al., 2010). A simple approach for gas/particle mass transfer used in some GCMs, such as CAM5 is to treat sulfate and ammonium only with a full neutralization (the NH_4^+/SO_4^{2-} molar ratio of 2 for a mode) through an irreversible condensation.

In this work, a comprehensive gas-phase chemical mechanism and detailed inorganic aerosol treatments for nucleation and aerosol thermodynamics are incorporated into CAM version 5.1 (CAM5.1) in the CESM version 1.0.5 (CESM1.0.5). Several modifications are also made to the existing treatments such as condensation and aqueous-phase chemistry. The objectives are to improve the representations of gas-phase chemistry and inorganic aerosol treatments in CESM/CAM5.1, and reduce associated uncertainties. The improved model with

enhanced capabilities can be applied for decadal simulations to study interactions among atmospheric chemistry, aerosols, and climate change.

2. Model Development and Improvement

CESM is a fully-coupled global Earth system model, which includes land, ocean, atmosphere, and sea ice components. The atmosphere component used in this study is CAM5.1. Existing and new model treatments related to this study are described in this section. Further details on CAM5.1 can be found at http://www.cesm.ucar.edu/models/cesm1.0/cam/.

2.1 Existing Gas-Phase Chemistry and Aerosol Treatments in CESM/CAM5.1

CAM5.1 uses a simple gas-phase chemistry for sulfur species, which includes 1 photolytic reaction and 7 kinetic reactions among 6 gas-phase species (i.e., hydrogen peroxide (H_2O_2), sulfuric acid (H_2SO_4), sulfur dioxide (SO_2), dimethylsulfide (DMS), ammonia (NH_3), and semi-volatile organic gas (SOAG)). A more comprehensive gas-phase mechanism with 40 photolytic reactions and 172 kinetic reactions among 103 species, i.e., the Model of OZone and Related chemical Tracers version 4 (MOZART-4) of Emmons et al. (2010), has been incorporated into the official released CAM5.1. It was only coupled with the bulk aerosol module (BAM) in CAM5.1 implemented in CESM 1.0.5 that is used in this work (It was coupled with MAM in CESM v1.1). In addition to BAM, CAM5.1 contains the modal aerosol model (MAM) that is based on modal representations of aerosols. In this study, MAM is used because it can represent more accurate size distributions as compared to BAM. There are two versions of MAM, one with seven lognormal modes (MAM7), and the other with three lognormal modes (MAM3) (Liu et al., 2012), and both are coupled with the simple gas-phase chemistry in the

default model. MAM7 is used in this study because it contains explicit treatments for ammonium and size distributions for dust, sea-salt, and primary carbon compared to MAM3. MAM7 explicitly treats sulfate, ammonium, sea-salt, dust, BC, POM, and SOA. It simulates condensational growth of aerosol, nucleation, coagulation, dry deposition, wet removal, and water uptake. Condensation is simulated based on a kinetic approach, in which MAM7 treats H_2SO_4, NH_3, and methanesulfonic acids (MSA) as completely non-volatile species and treats SOAG as a volatile species, using a constant accommodation coefficient of 0.65 for all these condensing species based on Adams and Seinfeld (2002). NH_3 condensation stops when the NH_4^+/SO_4^{2-} molar ratio of a particle mode reaches 2 (i.e., fully neutralized by SO_4^{2-} ions). The net uptake rate, I_{net}, due to gas to particle mass transfer for each species to each mode is simulated as,

$$I_{net} = \int dx \frac{dN}{dx} I_{cond} \quad (1)$$

$$I_{cond} = 2 \times \pi \times D_g \times D_p \times F(Kn, \alpha) \quad (2)$$

$$F(Kn, \alpha) = \frac{0.75 \times (1 + Kn)}{Kn \times \left(\frac{1 + Kn}{\alpha} + 0.283 \right) + 0.75} \quad (3)$$

where D_p is the particle diameter; x is the logarithmic diameter of particle, = $ln(D_p)$; dN/dx is the log-normal particle number density distribution; I_{net} is the gas condensation rate; Kn is the Knudsen number; α is the accommodation coefficient of condensable vapor; D_g is the gas diffusivity, and F(Kn, α) is the Fuchs-Sutugin correction factor that describes the resistance to uptake caused by gas-phase diffusion. Equation (1) is solved using the Gauss-Hermite quadrature of order 2. Based on equation (3), as α approaches zero, F(Kn, α) approaches zero. Consequently, I_{cond} (i.e., the uptake rate) approaches zero in equation (1).

There are three nucleation parameterizations in MAM7. The empirical power law of Wang and Penner (2009) (WP09) is used in the planetary boundary layer (PBL), which includes a first-order dependence on H_2SO_4 vapor with a prefactor of 1×10^{-6}. The binary H_2SO_4-H_2O homogeneous nucleation of Vehkamaki et al. (2002) (VE02) and ternary H_2SO_4-NH_3-H_2O homogeneous nucleation of Merikanto et al. (2007) (ME07) are used above PBL. MAM7 also only considers the neutralization of SO_4^{2-} by NH_4^+ during condensational growth. A more detailed description of MAM can be found in Liu et al. (2012).

2.2 New and Modified Model Treatments Implemented in This Work

2.2.1 Gas-Phase Chemical Mechanism

Highly simplified gas-phase mechanism as used in default CAM5.1 can result in large uncertainties in the predictions of oxidants and gaseous precursors for secondary aerosols. Therefore, a new gas-phase mechanism, the 2005 Carbon Bond Mechanism for Global Extension (CB05_GE) (Karamchandani et al., 2012) has been implemented into CAM5.1 using the same chemical preprocessor as MOZART-4 (Lamarque et al., 2012) and coupled with both MAM3 and MAM7. CB05_GE was developed to simulate major chemical reactions for global-through-urban applications as illustrated in Zhang et al. (2012b). A more detailed description of CB05_GE can be found in Karamchandani et al. (2012). In this study, gas precursors for SOA in CB05_GE are mapped to SOAG to make it compatible in MAM7. As the first study of CESM/CAM5.1 with CB05_GE, this work focuses on the impact of gas-phase chemistry. The heterogeneous chemistry on the surface of aerosol is turned off. CB05_GE implemented in CESM/CAM5 contains a total of 273 reactions including 50 photolytic reactions and 223 kinetic

reactions among 93 gas-phase species in this study. The gas-phase chemical system is solved using an implicit backward Euler method.

2.2.2 Ion-mediated nucleation parameterization

Ions generated by cosmic radiation and natural radioactive decay have been studied for a long time as an important source to enhance nucleation (Raes et al., 1986). An IMN model is developed by Yu (2010) (Yu10) for H_2SO_4-H_2O system, and explicitly solves the dynamic equations in terms of temperature, RH, H_2SO_4 vapor concentration, ionization rate, and surface area of preexisting particles. Different from classic binary nucleation theory, which is based on the minimization of changes in Gibbs free energy (Seinfeld and Pandis, 2006), IMN is based on a kinetic model that considers the interactions among ions, neutral and charged clusters, vapor molecules, and preexisting particles (Yu, 2010). The global ionization rates due to cosmic rays are calculated based on the schemes given in Usoskin and Kovaltsov (2006) and the contribution of radioactive materials from soil to ionization rates is parameterized based on the profiles given in Reiter (1992). To reduce the computing cost using IMN in 3-D models, Yu et al. (2008) developed lookup tables with simple interpolation subroutines to calculate nucleation rates under typical atmospheric conditions. In this work, IMN based on YU10 is implemented into MAM7 and combined with default nucleation parameterizations (VE02, ME07, and WP09) in order to improve the J predictions and aerosol number concentrations in upper troposphere. The J value above PBL is taken as the maximum value among predictions from IMN (YU10) and homogeneous nucleation (VE02 or ME07), and the J value within PBL is taken as the maximum value among predictions from IMN (YU10), homogeneous nucleation (VE02 or ME07), and the first-order parameterization (WP09).

227

228 2.2.3 Inorganic Aerosol Thermodynamics

229 Gas-particle partitioning is an important process in the formation and evolution of
230 secondary aerosols. Several factors affect gas-particle partitioning, such as temperature, RH,
231 saturation vapor pressures of species, the physical state of the condensed-phase, and the
232 interactions among aerosol components (Zuend et al., 2010). Most models focus on inorganic
233 aerosols. Fountoukis and Nenes (2007) developed a computationally-efficient thermodynamics
234 equilibrium model, ISORROPIA II, for the magnesium (Mg^{2+}) - potassium (K^+) - calcium (Ca^{2+})
235 - NH_4^+- Na^+ - SO_4^{2-}- NO_3^-- Cl^-- H_2O aerosol system. An important difference between
236 ISORROPIA II and most other thermodynamics equilibrium models is that ISORROPIA II
237 simulates crustal species, such as Mg^{2+}, K^+, and Ca^{2+}, which are important constituents of
238 atmospheric aerosols, in particular, mineral dust. Therefore, to explicitly simulate aerosol
239 thermodynamics, ISORROPIA II has been implemented into MAM7 and applied for
240 accumulation, Aitken, fine sea-salt, and fine dust modes to explicitly simulate thermodynamics
241 of SO_4^{2-}, NH_4^+, NO_3^-, Cl^-, and Na^+ as well as the impact of crustal species associated with fine
242 dust modes on aerosol thermodynamics. The concentrations of K^+, Ca^{2+}, and Mg^{2+} as the input
243 for ISORROPIA II are calculated from dust concentrations, using the mass ratios of 1.022×10^{-3},
244 1.701×10^{-3}, and 7.084×10^{-4}, respectively (Van Pelt and Zobeck, 2007). The resulted
245 concentrations of aerosol components from ISORROPIA are mapped back to fine aerosol modes
246 based on their mass ratios to the total mass over all fine modes at the previous time step.

247 Aerosol thermodynamics involving coarse particles (in coarse sea-salt and dust modes) is
248 currently not treated explicitly in this work, given the high computational cost (by at least a
249 factor of 3) for solving the non-equilibrium system involving coarse particles. Instead, the simple

kinetic approach used in the default CAM5.1 is used to simulate the condensation of inorganic gases onto coarse modes (see section 2.2.4). For fine mode particles, before thermodynamic calculation using ISORROPIA II, the condensation and nucleation processes are simulated to allow a more realistic allocation of gaseous H_2SO_4 between these two competing processes. Such a treatment for fine mode particles is similar to the kinetic approach used in regional air quality models, except that the condensation is assumed to be irreversible with lower limit values of mass accommodation coefficients in this work.

2.2.4 Modifications of Existing Aerosol Treatments

MAM 7 does not treat NO_3^- and it treats NaCl as one species. In this work, MAM7 is modified to explicitly simulate NO_3^-, Cl^-, and Na^+ using a similar method to the condensation of H_2SO_4 and NH_3. NO_3^- and Cl^- are simulated in all modes except for primary carbon mode. Na^+ is simulated in sea-salt modes. The source of Na^+ is calculated based on the mass ratio of Na and Cl from sea-salt emissions. The source of Cl^- includes sea-salt emissions, and the condensation of HCl resulted from HCl emissions and gas-particle partitioning of total chloride.

Species-dependent accommodation coefficients are used for H_2SO_4, NH_3, HNO_3, and HCl, with the values of 0.02, 0.097, 0.0024, and 0.005 (Zhang et al., 1998; Sander et al., 2002), respectively. Since by default the model treats the condensation of inorganic volatile gas species as irreversible process (no evaporation) (see equation (1)), the lower limit values of mass accommodation coefficients are used for these species to represent their net fluxes from the gas-phase to the liquid/solid phases. Such lower limit values correspond to uptake coefficients, which represent the net fluxes and are smaller than mass accommodation coefficients. To ensure electroneutrality in each mode after kinetically condensing H_2SO_4, NH_3, HNO_3, and HCl at different condensation (or uptake) rates, the condensation of NH_3 will stop when the mole

concentration of cations (i.e., NH_4^+) is equal to sum of those of anions (i.e., $[NH_4^+] = 2\times[SO_4^{2-}]+[NO_3^-]+[Cl^-]$). While such an approach allows the gas/particle portioning of those volatile species over both fine and coarse modes, the irreversible condensation with lower limit mass accommodation coefficients assumed in this work, however, may contribute to model biases in simulating condensation of volatile species on coarse mode particles. A more accurate method (i.e., reversible condensation) should be used for volatile species for future work. The original MAM7 treats NH_3(g)/NH_4^+ in cloud water. In this work, the dissolution and dissociation of HNO_3 and HCl to produce NO_3^- and Cl^- in cloud water are added in the model based on Marsh and McElroy (1985) and Seinfeld and Pandis (2006), i.e.,

$$\boldsymbol{HNO_{3\,(g)} \rightleftharpoons HNO_3(aq) \rightleftharpoons H^+ + NO_3^-}$$
$$\boldsymbol{HCl_{(g)} \rightleftharpoons HCl_{(aq)} \rightleftharpoons H^+ + Cl^-}$$

The concentration of H^+ (thus the pH value of the solution) is obtained by solving the electro-neutrality equation using the bisection method. The aqueous-phase chemical system is solved analytically.

3. Model Configurations and Evaluation Protocols

3.1 Model Setup and Simulation Design

Table 1 summarizes the CESM/CAM5.1 simulations that are designed to examine the impacts of individual new and modified treatments on model predictions. The first set of simulations includes two simulations with the same default MAM7 coupled with different gas-phase mechanisms: one uses the simple gas-phase chemistry (MAM_SIM) with a total of 37 prognostic species and one uses the CB05_GE (MAM_CB05_GE) with a total of 127 prognostic

295 species. A comparison of the two simulations provides an estimate of the impacts of gas-phase
296 chemical mechanisms. The second set of simulations consists of five simulations that use the
297 same CB05_GE gas-phase mechanism but with modified and new aerosol treatments
298 individually and jointly. The first one is MAM_CON that uses an explicit treatment for NO_3^-, Cl^-,
299 and Na^+ and species-dependent mass accommodation coefficients for condensation and that
300 includes the aqueous-phase chemistry of HNO_3/NO_3^- and HCl/Cl^-. This simulation includes a
301 total of 139 prognostic species. The second one is MAM_CON/IMN that uses the same
302 treatments as MAM_CON but with IMN as one of the nucleation mechanisms and a prefactor of
303 1.0×10^{-8} in WP09. The third one is MAM_CON/ISO that uses the same treatments as
304 MAM_CON but with ISORROPIA II for aerosol thermodynamics assuming metastate
305 equilibrium (i.e., liquid only). The fourth one is MAM_NEWA that uses the same treatments as
306 MAM_CON but with all new and modified aerosol treatments and a prefactor of 1.0×10^{-9} for
307 WP09. The fifth one is MAM_NEWB that uses the same treatments as MAM_NEWA, but with
308 ISORROPIA II assuming a stable condition (i.e., solid and liquid coexist). A comparison of
309 MAM_CB05_GE with MAM_CON indicates the impact of modified condensation and aqueous-
310 phase chemistry. A comparison of MAM_CON/IMN, MAM_CON/ISO, and MAM_NEWA with
311 MAM_CON indicates the impacts of IMN, ISORROPIA II, and combined new and modified
312 aerosol treatments, respectively. Comparison of MAM_NEWB with MAM_NEWA indicates the
313 impacts of thermodynamic conditions on gas-aerosol partitioning. The 3rd set of simulation
314 includes one simulation using the same configuration as MAM_NEWA but with adjusted
315 emissions (MAM_NEW/EMIS). Its comparison with MAM_NEWA indicates the impacts of
316 uncertainties in emissions on model predictions. The 4th set of simulation includes one simulation
317 using the same configuration as MAM_SIM but with prescribed SST for a 5-yr period during

2001-2005 (MAM_SIM_5Y), and two simulations both using the same configuration as MAM_NEW/EMIS for 2001-2005, but one with prescribed SST (MAM_NEW_5YA), and the other in a fully-coupled mode (MAM_NEW_5YB).

All these simulations use the same approach for photolytic rates calculations based on Lamarque et al. (2012), the same aqueous-phase chemistry of Barth et al. (2000), and the same physical options as those in MAM_SIM. Major physical options include the cloud microphysics parameterization of Morrison and Gettelman (2008), the moisture PBL scheme of Bretherton and Park (2009), the shallow convection scheme and deep convection scheme of Park and Bretherton (2009) and Zhang and McFarlane (1995), respectively, the aerosol activation parameterization of Abdul-Razzak and Ghan (2000), and the Rapid Radiative Transfer Model for GCMs (RRTMG) of Iacono et al. (2003, 2008) for long and short-wave radiation. The land surface processes are simulated by the Community Land Model (CLM) of Lawrence et al. (2011) in CESM that is coupled with CAM5.1.

All simulations except for MAM_SIM_5Y and MAM_NEW_5YA are performed with fully-coupled CESM1.0.5 with standard B_1850-2000_CAM5_CN configuration, which represents 1850 to 2000 transient conditions and includes all active components in CESM with biogeochemistry in the land model. MAM_SIM_5Y and MAM_NEW_5YA are performed with standard F_AMIP_CAM5 configuration, which uses a climatological dataset for SST provided by NCAR for ocean model. The simulations are conducted for the full-year of 2001 and 2001-2005 at a horizontal resolution of $0.9^{o}\times1.25^{o}$ and a vertical resolution of 30 layers for CAM5.1. The initial conditions for ice and ocean models are from CESM default settings. The initial conditions for the land model are based on the output from the NCAR's CESM/CAM4 B_1850-2000_CN simulation. The initial conditions for CAM5 are derived from a 10-yr (1990-2000)

CAM5 standalone simulation with the MOZART chemistry provided by NCAR. A 1-year (January 1-December 31, 2000) CESM/CAM5 simulation using NCAR's CESM B_1850-2000_CAM5_CN component set is performed as spinup to provide the initial conditions for meteorological variables and chemical species that are treated in both MOZART and CB05_GE. An additional 3-month (October 1-December 31, 2000) CESM/CAM5 simulation based on a 10-month (January-October, 2000) CESM/CAM5 output using initial conditions from NCAR's CESM B_1850-2000_CAM5_CN is performed as spinup to provide initial conditions for chemical species that are treated in CB05_GE but not in MOZART. All production simulations of 2001 are from January 1 - December 31, 2001 and those of 2001-2005 are from January 1, 2001- December 31, 2005. The offline anthropogenic emissions used in all simulations except for MAM_NEW/EMIS are taken from Zhang et al. (2012b) (see Table 2 of Zhang et al. (2012b) for the sources of those anthropogenic emissions). Anthropogenic emissions used in MAM_NEW/EMIS are adjusted emissions based on those of Zhang et al. (2012b), with adjustment factors of 0.7, 0.5, and 1.2 for SO_2 over CONUS, Europe, and Asia, respectively, and 1.2 for NH_3, BC, and organic carbon (OC), and 1.3 for carbon monoxide (CO) over all three regions. Those emissions are adjusted based on the comparison with the emission inventories from the Representative Concentration Pathways (RCPs), the MOZART version 4 (MOZART-4), the Reanalysis of the TROpospheric chemical composition (RETRO), the Global Fire Emissions Database (GFED) version 2, and preliminary evaluation of CESM/CAM5.1 with modified and new gas and aerosol treatments using available observations. The online emissions include biogenic volatile organic carbon (Guenther et al., 2006), mineral dust (Zender et al., 2003), and sea-salt (Martensson et al., 2003).

364 3.2 Available Measurements for Model Validation

365 A number of observational datasets from surface networks and satellites are used for
366 model evaluation. They are summarized along with the variables to be evaluated in Table A1 in
367 the supplementary material. Global surface networks include the Baseline Surface Radiation
368 Network (BSRN) and the National Oceanic and Atmospheric Administration Climate
369 Diagnostics Center (NOAA/CDC). The satellite datasets include the Moderate Resolution
370 Imaging Spectroradiometer (MODIS), the Clouds and Earth's Radiant Energy System (CERES),
371 the Total Ozone Mapping Spectrometer/the Solar Backscatter UltraViolet (TOMS/SBUV), the
372 Measurements Of Pollution In The Troposphere (MOPITT), and the Global Ozone Monitoring
373 Experiment (GOME). Other satellite-based data include the MODIS-derived CDNC from
374 Bennartz (2007) (BE07).

375 Regional observational networks include the Clean Air Status and Trends Network
376 (CASTNET), the Interagency Monitoring of Protected Visual Environments (IMPROVE), and
377 the Speciation Trends Network (STN) over CONUS; the European Monitoring and Evaluation
378 Program (EMEP), the Base de Données sur la Qualité de l'Air (BDQA), and the European air
379 quality database (AirBase) over Europe; the Ministry of Environmental Protection of China
380 (MEP of China), the National Institute for Environmental Studies of Japan (NIES of Japan), and
381 Taiwan Air Quality Monitoring Network (TAQMN) over East Asia. The observational data for
382 particle formation rate J is compiled from Kulmala et al. (2004) and Yu et al. (2008), which
383 include land-, ship-, and aircraft-based measurements.

384

385 3.3 Evaluation Protocol

386 The protocols for performance evaluation include spatial distributions and statistics,
387 following the approach of Zhang et al. (2012b). The analysis of the performance statistics will
388 focus on mean bias (MB), normalized mean bias (NMB), normalized mean error (NME), and
389 root mean square error (RMSE). The radiative variables are evaluated annually, including
390 downwelling shortwave radiation (SWD) and downwelling longwave radiation (LWD) from
391 BSRN; outgoing longwave radiation (OLR) from NOAA/CDC; shortwave cloud forcing
392 (SWCF) from CERES; cloud fraction (CF), aerosol optical depth (AOD), cloud optical thickness
393 (COT), cloud water path (CWP), precipitating water vapor (PWV), and CCN from MODIS; as
394 well as CDNC from BE07. Chemical concentrations evaluated include seasonal and annual
395 averaged concentrations of CO, O_3, SO_2, NH_3, NO_2, HNO_3, PM, and its major components (i.e.,
396 SO_4^{2-}, NO_3^-, and NH_4^+, BC, OC, total carbon (TC) for CONUS and Europe). The chemical
397 observations over East Asia are very limited, and they only include surface concentrations of CO,
398 SO_2, NO_2, O_3, and PM_{10}. Column concentrations of tropospheric CO and NO_2, and tropospheric
399 O_3 residual (TOR) are evaluated for globe.
400 All observational data used for evaluating 2001 simulations are based on 2001 only
401 except for particle formation rates (J) that are based on different years compiled from Kulmala et
402 al. (2004) and Yu et al. (2008). All observational data used for evaluating 2001-2005 simulations
403 are based on 2001-2005.
404
405 **4. Model Evaluation for MAM_SIM Based on Original Model Treatments**
406 Tables 2 and 3 show MBs and NMBs of radiative/cloud and chemical predictions,
407 respectively. The model performance of the baseline simulation, MAM_SIM, is discussed below,
408 and that for all other simulations will be discussed in section 5.

As shown in Table 2, radiative variables such as LWD and SWD are underpredicted by 3.4 W m^{-2} (~ -1.1%) and 2.0 W m^{-2} (~ -1.1%), respectively, whereas OLR and SWCF are overpredicted by 8.8 W m^{-2} (~ 4.1%) and 3.2 W m^{-2} (~ 7.9%) respectively. Cloud variables such as CF and PWV are slightly underpredicted, whereas COT, CWP, column CCN at a supersaturation of 0.5% (CCN5), and CDNC are largely underpredicted, with NMBs of -77.8% to -55.6%, which is likely due to the limitations in the current model treatments of cloud microphysics and aerosol-cloud interactions in CAM5.1.

AOD is also underpredicted by 36.1%, which is likely due to inaccurate predictions of aerosol concentrations and uncertainties in the assumed hygroscopicity of aerosol components in the calculation of optical properties and water uptake. For example, as shown in Table 3, $PM_{2.5}$ concentrations over CONUS and Europe, and PM_{10} concentrations over CONUS, Europe, and East Asia are underpredicted, with NMBs of -67.5% to -31.8%, which is due to the inaccurate predictions of SO_4^{2-}, NH_4^+, and organic aerosols, and missing major inorganic aerosol species such as nitrate and chloride. The concentrations of BC, OC, and TC are underpredicted (by ~ 50%), which is likely due to the uncertainties in the BC and primary OC emissions as well as treatments for SOA formation. In particular, the SOA treatment used in CAM5.1 is based on a highly-simplified aerosol yield approach with a single lumped semi-volatile organic gas (i.e., SOAG). For gaseous species, SO_2 concentrations over CONUS and Europe are significantly overpredicted by 10.3 μg m^{-3} (~ 264.8%) and 6.6 μg m^{-3} (~ 97.5%), respectively, whereas SO_2 concentrations over East Asia are largely underpredicted by 7.9 μg m^{-3} (by ~63.0%). NH_3 concentrations over Europe are also largely underpredicted by 82.0%. These large biases in SO_2 and NH_3 are likely due in part to the uncertainties in the emissions of SO_2 and NH_3, which in turn affect the predictions of SO_4^{2-} and NH_4^+. The J values in PBL are highly underpredicted by

99.6%, which is mainly due to the inaccurate calculation of H_2SO_4 vapor concentration that participates in the nucleation and uncertainties in the nucleation parameterizations used in the default CESM/CAM5.1.

5. Sensitivity Simulations

5.1 Impacts of New Gas-Phase Chemistry

Compared to simple gas-phase chemistry, many more gaseous species and chemical reactions simulated in CB05_GE can affect secondary aerosol formation through gas-to-particle mass transfer and aqueous-phase chemistry and affect climatic variables through chemistry feedbacks to the climate system. Figure 1a shows the absolute differences of H_2O_2, SO_2, SO_4^{2-}, and SOA between MAM_CB05_GE and MAM_SIM. MAM_CB05_GE treats more gaseous species and chemical reactions than MAM_SIM, leading to large changes in the concentrations of gaseous and PM species. Compared with MAM_SIM, MAM_CB05_GE predicts higher H_2O_2 by 0.4 ppb, SO_2 by 7.3 ppt, SO_4^{2-} by 0.01 μg m^{-3}, and SOA by 0.06 μg m^{-3} in terms of global mean. Those changes are mainly caused by different gas-phase chemical mechanisms used in MAM_SIM and MAM_CB05_GE. While MAM_CB05_GE explicitly simulates OH, HO_2, NO_3, and O_3, MAM_SIM uses climatology data for these species. OH simulated by MAM_CB05_GE is lower than that prescribed by MAM_SIM by up to 2.8×10^6 molecules cm^{-3}, or higher by up to 3.0×10^6 molecules cm^{-3} in different regions (Figure not shown), with a higher global mean by MAM_CB05_GE. MAM_SIM includes the production of H_2O_2 from the self-destruction of HO_2 and the loss of H_2O_2 through its photolytic reaction and its reaction with OH. Higher H_2O_2 in MAM_CB05_GE is mainly due to greater production of H_2O_2 from additional chemical reactions (e.g., OH+OH) than loss of H_2O_2 through the reactions of OH + H_2O_2, O + H_2O_2, Cl +

455 H_2O_2, and Hg + H_2O_2. Different predictions in H_2O_2 can in turn affect OH mixing ratios in
456 MAM_CB05_GE but not in MAM_SIM. In addition, the photolytic reactions of VOCs (e.g.,
457 HCHO, peroxyacyl nitrates (PAN), and peroxyacetic and higher peroxycarboxylic acids (PACD))
458 and other gases (e.g., HNO_3, HONO, HNO_4, HOCl, and HOBR) treated in MAM_CB05_GE can
459 produce OH. Figure 1b shows the absolute differences between the mixing ratios of major
460 oxidants predicted from MAM_CB05_GE and climatology values used in MAM_SIM. The
461 global mean mixing ratios of oxidants are higher in MAM_CB05_GE than climatology data in
462 MAM_SIM, leading to more oxidation of VOCs and therefore more SOA in MAM_CB05_GE.
463 Higher O_3 predicted from MAM_CB05_GE over most of the domain is mainly due to more O_3
464 precursors (e.g., NO_2 and VOCs) treated in the model. Despite higher OH mixing ratios in
465 MAM_CB05_GE, many gaseous species such as NO_x, SO_2, HNO_3, HONO, and other VOCs are
466 oxidized by OH to form secondary inorganic and organic aerosols. Those oxidation reactions
467 compete for limited OH, leading to less oxidation of SO_2, thus higher SO_2 mixing ratios over
468 most land areas by MAM_CB05_GE. Lower SO_2 mixing ratios over the oceanic areas in
469 MAM_CB05_GE is due to the combined effects of less production of SO_2 from lower DMS
470 mixing ratios (due to increased OH levels) and greater SO_2 oxidation from higher OH mixing
471 ratios.

472 The changes in the concentrations of PM and its components are due to the change in the
473 mixing ratios of gaseous precursors. CB05_GE contains more photolytic reactions, which affect
474 the mixing ratios of OH, SO_2, and H_2SO_4, and subsequently the concentration of SO_4^{2-} through
475 condensation and homogeneous nucleation. Higher SO_2 mixing ratios in MAM_CB05_GE result
476 in more H_2SO_4 thus more SO_4^{2-}. For example, both SO_2 mixing ratios and SO_4^{2-} concentrations
477 are higher over eastern China in MAM_CB05_GE. More SO_4^{2-} over the oceanic areas is mainly

478 due to more oxidation of SO_2 by OH. Due to the simplification of aerosol thermodynamics in
479 default MAM7, the concentrations of SO_4^{2-} can affect the concentrations of NH_4^+ directly and
480 therefore NH_3 mixing ratios and PM number concentrations (PM_{num}). For example, the increase
481 of SO_4^{2-} results in an increase in NH_4^+ and PM_{num}, and a decrease in NH_3. The increase of SO_4^{2-}
482 and PM_{num} can increase AOD, CF, COT, CWP, PWV, and CDNC and therefore affect radiation
483 by increasing LWD and SWD (Figures not shown, see changes in performance statistics of these
484 affected variables in Table 2). The increase of SOA is due to the inclusion of more gaseous
485 precursor emissions (e.g., isoprene, terpene, xylene, and toluene) in MAM_CB05_GE, which
486 contribute to SOAG and thus SOA through gas-to-particle conversion.
487 Figure 2 shows the spatial distributions of CO, O_3, NO_2, HNO_3, hydrochloric acid (HCl),
488 and isoprene (ISOP) that can be predicted by MAM_CB05_GE but not by MAM_SIM. CO
489 mixing ratio is higher in most Asia, central Africa, South Africa, and eastern U.S., which is
490 mainly due to higher CO emissions in those regions and the production of CO from the
491 photolytic reactions of VOCs (e.g., formaldehyde, acetaldehyde, and isoprene). Higher O_3
492 mixing ratios in the northern hemisphere than southern hemisphere are mainly due to much
493 higher mixing ratios of O_3 precursors. Higher O_3 mixing ratios over Mediterranean Sea are
494 mainly due to the transport of O_3 and its precursors from source regions and less deposition onto
495 ocean surface. Higher O_3 mixing ratios over Tibet are mainly due to the stratospheric influences
496 from high altitude and no titration of O_3 due to low NO mixing ratios (< 0.2 ppb) in this region.
497 Higher mixing ratios of NO_2 over most Asia, eastern U.S, Europe, and Central Africa are mainly
498 due to higher NO_x emissions over those regions, which also result in higher HNO_3 in those
499 regions. Higher mixing ratios of HCl over Europe, India, and East Asia are mainly due to the
500 higher anthropogenic HCl emissions in those regions. In addition, MAM_CB05_GE includes

501 oceanic emissions of HCl, leading to higher HCl over ocean. Higher isoprene mixing ratios over
502 South Africa, central Africa, and Oceania are mainly due to higher isoprene emissions in those
503 regions, which also contribute to the formation of SOA in those regions.
504 The aforementioned changes in the concentrations of gaseous species and PM due to new
505 gas-phase chemistry implemented in the model and its feedbacks to radiation through the climate
506 system result in a change in predicted cloud properties and radiation balance that in turn affect
507 the predictions of all chemical species during subsequent time steps. As a consequence of
508 interwoven changes due to complex feedback mechanisms, the two simulations perform
509 differently, with noticeable improvement by MAM_CB05_GE. As shown in Table 2, compared
510 with MAM_SIM, MAM_CB05_GE reduces MB of LWD by 17.6%, OLR by 8.0%, CF by
511 28.6%, COT by 1.0%, PWV by 28.0%, AOD by 5.5%, and CDNC by 1.8%, leading to 0.3-2.2%
512 absolute reduction in their NMBs. Although MAM_CB05_GE increases MB of SWD by 26.2%,
513 the increases in their NMBs are only 1.2%. As shown in Table A1 in the supplementary material,
514 the changes in most cloud and radiative variables between MAM_SIM and MAM_CB05_GE are
515 statistically significant. As shown in Table 3, MAM_CB05_GE also reduces MBs of SO_2 by
516 2.5% and PM_{10} by 8.1% over East Asia, NH_3 by 1.3% and SO_4^{2-} by 12.5% over Europe, OC by
517 11.1%, TC by 8.3%, and $PM_{2.5}$ by 3.3% over CONUS, leading to 0.8-6.5% absolute reductions
518 in NMBs. Despite the model improvement by CB05_GE, large biases still remain for some
519 chemical species. For example, CO over East Asia is largely underpredicted with an NMB of -
520 82.1% (see Table 3), which results from the uncertainties in the CO emissions over East Asia.
521 However, the column CO over globe is predicted very well, with an NMB of -5.7%. Large biases
522 in SO_2 predictions over CONUS, Europe, and East Asia are mainly due to the uncertainties in the
523 SO_2 emissions over those regions. Large biases in O_3 over Europe are likely due to the

524 uncertainties in the O_3 precursor emissions (e.g., NO_x) and inaccurate predictions of radiation
525 over Europe. In particular, the large underpredictions in NO_2 concentrations (likely due to the
526 uncertainties in the NO_x emissions and overpredictions in radiation, see section 5.5 for more
527 detailed discussions) indicate insufficient NO_x for titration of O_3, leading to a large
528 overprediction in O_3 concentrations in Europe. The large biases in HNO_3 are due to no treatment
529 for gas-particle partitioning in both simulations.
530
531 5.2 Impacts of Condensation and Aqueous-Phase Chemistry
532 The mass accommodation coefficient (α) for H_2SO_4 vapor is subject to considerable
533 uncertainty. The default condensation module with a default α value of 0.65 gives a very low
534 concentration of H_2SO_4, resulting in very low nucleation rates and aerosol number
535 concentrations. Considering that the original model treats H_2SO_4 and NH_3 condensation as an
536 irreversible process, the default α value of 0.65 for H_2SO_4 and NH_3 is reduced to 0.02 and 0.097,
537 respectively, based on Zhang et al. (1998). This change in α value provides sufficient H_2SO_4 and
538 NH_3 for nucleation with a typical H_2SO_4 concentration range of 10^6~10^8 molecules cm^{-3}.
539 Because HNO_3 and HCl are semi-volatile species, the lower limits of α (0.0024 and 0.005,
540 respectively) based on Sander et al. (2002) are selected for their irreversible condensation
541 process. NH_4^+ from NH_3 condensation will be constrained by the available SO_4^{2-}, NO_3^-, and
542 condensed Cl^- to neutralize the system.
543 Figure 3 shows the absolute differences of NH_3, SO_2, HNO_3, HCl, H_2SO_4, total
544 particulate ammonium (TNH_4), total particulate sulfate (TSO_4), total particulate nitrate (TNO_3),
545 and total particulate chloride (TCL) in all the modes except primary carbon mode, and $PM_{2.5}$
546 between MAM_CON and MAM_CB05_GE in June, July, and August (JJA), 2001. Due to the

547 inclusion of HNO_3 and HCl condensation in MAM_CON, the concentrations of HNO_3 and HCl
548 decrease by 0.1 ppb (~72%) and 0.097 ppb (~84%), respectively. NO_3^- is not simulated in the
549 original model and the concentration of NO_3^- is assumed as zero in MAM_CB05_GE. Therefore,
550 the concentration of NO_3^- increases due to the condensation of HNO_3 in MAM_CON. The
551 concentration of TCL in MAM_CB05_GE is calculated from the mass ratio of chloride in sea-
552 salt. Over land, TCL increases significantly due to the condensation of HCl to form Cl^-. The
553 change of TCL over ocean is mainly due to the change of sea-salt emissions. The changes of SO_2
554 mixing ratios are mainly due to the differences in mixing ratios of species in sulfur chemistry in
555 the two simulations. For example, compared to MAM_CB05_GE, the increase of SO_2 over
556 eastern U.S. in MAM_CON is likely due to less SO_2 oxidation in clouds (Figure not shown),
557 which results from lower CF. The decrease of SO_2 mixing ratios over most oceanic areas is likely
558 due to the combined effects of DMS oxidation and SO_2 oxidations in MAM_CON. More SO_2
559 can result in more H_2SO_4 and therefore more SO_4^{2-} through condensation and homogeneous
560 nucleation of H_2SO_4. The changes in H_2SO_4 concentrations are the results of changes of SO_2
561 mixing ratios. The mass accommodation coefficient of H_2SO_4 is reduced significantly (by a
562 factor of 32.5), allowing more H_2SO_4 to participate in binary/ternary homogeneous nucleation
563 and produce more secondary SO_4^{2-}, improving predictions of SO_4^{2-} over CONUS but degrading
564 the performance of SO_4^{2-} over Europe (see Table 3). Although the mass accommodation
565 coefficient of NH_3 is reduced significantly (by a factor of 67), more available NH_3 can participate
566 in the ternary homogeneous nucleation and produce secondary NH_4^+. Meanwhile, the secondary
567 NH_4^+ formed from NH_3 condensation is also constrained by available SO_4^{2-}, NO_3^-, and
568 condensed Cl^-. As a result, the concentrations of NH_3 decrease and those of NH_4^+ increase. Due
569 to more available H_2SO_4 participating in the nucleation, J has been improved significantly,

570 reducing the NMB from -99.5% to -12.8%. With an inclusion of the dissolution and dissociation
571 of HNO_3 and HCl in cloud water, more NH_3 is required to dissolve to maintain cation-anion
572 equilibrium in the cloud water, which further reduces the mixing ratios of NH_3, HNO_3, and HCl.
573 As shown in Table 3, compared with MAM_CB05_GE, MAM_CON gives better
574 performance against observations in terms of CO, NO_2, O_3, HNO_3, $PM_{2.5}$, and PM_{10} over Europe,
575 CO and PM_{10} over East Asia, O_3, HNO_3, SO_4^{2-}, NH_4^+, BC, OC, TC, and $PM_{2.5}$ over CONUS, and
576 column CO, column NO_2, TOR, and J over globe. As also shown in Table 2, the improved
577 chemical predictions improve the predictions of OLR, SWCF, CF, COT, CWP, AOD, and CDNC.
578 As shown in Table A1, the changes in most cloud /radiative variables between MAM_CB05_GE
579 and MAM_CON are statistically significant, indicating the significant impacts of the modified
580 condensation and aqueous-phase chemistry treatments on radiation. Treating condensation and
581 aqueous-phase chemistry of HNO_3 and HCl enables an explicit simulation of NO_3^- and Cl^- in
582 MAM7. However, the mass concentrations of SO_2 remain significant overpredictions, with
583 NMBs of 301.2% for CONUS, and 123.0% for Europe, mainly because of the uncertainties in
584 SO_2 emissions over those regions. Due to the simplified irreversible treatment for gas
585 condensation, the mass concentrations of SO_4^{2-}, NH_4^+, NO_3^-, and Cl^- are overpredicted, although
586 the lower limit of mass accommodation coefficient for each precursor is used in MAM_CON. As
587 shown in Table 3, the concentrations of SO_4^{2-}, NH_4^+, NO_3^-, and Cl^- from MAM_CON are
588 overpredicted by 1.7%, 20.0%, 198.2%, and 359.9%, respectively, for CONUS, and 40.3%,
589 85.0%, 67.8%, and 102.8%, respectively, for Europe. The large NMBs of NO_3^- and Cl^- in
590 MAM_CON are due to the small observed values for NO_3^- (i.e., 1.0 μg m^{-3} over CONUS and 2.0
591 μg m^{-3} over Europe) and Cl^- (i.e., 0.1 μg m^{-3} over CONUS and 0.7 μg m^{-3} over Europe), the

592 uncertainties in treating HNO_3 and HCl as non-volatile species using their lower limits of
593 accommodation coefficients, and lack of treatments for NO_3^- and Cl^- thermodynamics.
594
595 5.3 Impacts of New Particle Formation
596 Figure 4 shows the annual-mean vertical distributions of particle formation rate (J) values
597 and aerosol number concentrations, and simulated J values averaged between the ground level
598 and 1000-m overlaid with observations within the same layers. In MAM_CON/IMN, IMN is
599 combined with three default nucleation parameterizations to predict J throughout the atmosphere.
600 In MAM_CON, J over ocean is overpredicted by factors of 5-50, despite a seeming good NMB
601 of -12.8% in the globe mean (see Table 3). J values at several sites over land are underpredicted
602 by factors of 1-10, which compensates the large overpredictions at most sites over ocean. The
603 large underpredictions at those sites are likely due to the uncertainties in SO_2 emissions and
604 nucleation parameterizations, and the missing species that may have participated in nucleation.
605 For example, several other species may contribute to the new particle formation, including
606 methanesulfonic acid (van Dingenen and Raes, 1993), hydrochloric acid (Arstila et al., 1999),
607 organic compounds (Berndt, et al., 2013), iodine-containing compounds (Hoffmann et al., 2001),
608 and amines (Berndt et al., 2013). Limited observations also introduce some uncertainties in the
609 model validation. The overprediction of J over ocean is mainly due to the use of the prefactor of
610 1×10^{-6} in WP09. This prefactor is derived from limited in-situ measurements (Sihto et al., 2006).
611 It can vary by up to 3-4 orders of magnitude based on measurements in different areas and
612 seasons (Zhang et al., 2010), introducing a large uncertainty for its application to the global
613 scale. In MAM_CON/IMN, a prefactor of 1×10^{-8} is used in WP09 in PBL over the globe, which
614 then decreases J and aerosol number concentrations in PBL (see Figure 4). J in PBL is very

615 sensitive to the prefactor in WP09, and the uncertainty of the prefactor can result in a large bias
616 in predictions of J and aerosol number in PBL. With the implementation of IMN, J values in the
617 troposphere increase by factors of 2-10, which in turn increase the aerosol number concentrations
618 in the troposphere. Due to a stronger radiation in the upper layer, more available ions can
619 contribute to the new particle formation, therefore increasing the aerosol number concentrations
620 in the middle/upper troposphere and lower stratosphere by factors of 2-4.

621 Figure 5 shows the absolute differences of $PM_{2.5}$, AOD, column CCN5, CF, SWCF, and
622 SWD between MAM_CON and MAM_CON/IMN for 2001. Aerosol number can directly affect
623 CCN, which can affect cloud formation and properties as well as radiation. Changes of PM
624 concentrations also have impacts on AOD, CCN, CF, COT, and SWCF through both aerosol
625 direct and indirect effects. As a net result of all those interwoven changes initially triggered by
626 the increase of aerosol number concentrations in troposphere/stratosphere, AOD and column
627 CCN5 increase by 0.004 (or by 3.3%) and 2.1×10^{7} cm^{-2} (or by 11.9%), respectively, and SWCF
628 and SWD decrease by 0.1 W m^{-2} (or by 0.2%) and 0.8 W m^{-2} (or by 0.5%), respectively, in terms
629 of global mean. As shown in Table A1, the changes in SWD, AOD, and cloud variables such as
630 column CCN5, CDNC, and COT between MAM_CON and MAM_CON/IMN are statistically
631 significant, indicating the significant impacts of IMN on aerosol number concentration and cloud
632 prediction.

633 Compared with MAM_CON, IMN (MAM_CON/IMN) improves the predictions of SO_2,
634 NO_3^-, and $PM_{2.5}$ over CONUS, SO_2, SO_4^{2-}, NH_4^+, NO_3^-, Cl^-, $PM_{2.5}$, and PM_{10} over Europe, PM_{10}
635 over East Asia (see Table 3). The improved performance in aerosol concentrations and increased
636 aerosol numbers in the troposphere and lower stratosphere contribute to the improved
637 performance of aerosol and cloud parameters, with increased AOD, CCN, and CDNC, and

638 consequently increased CF, COT, CWP, and SWCF, as shown in Table 2. However, there are still
639 large biases for some chemical species predictions. For example, CO mixing ratio is
640 underpredicted over East Asia, which is mainly due to the uncertainty in CO emissions in this
641 region. Large biases in SO_2 predictions over CONUS, Europe, and East Asia are mainly due to
642 the uncertainties in SO_2 emissions in those regions. Large biases in NO_2 and HNO_3 predictions
643 over Europe are mainly due to the uncertainties in NO_x emissions and inaccurate predictions of
644 radiation over this region. The performance of J degrades with NMBs from -21.8% to -49.6% in
645 the globe, which is due to the use of a smaller prefactor of WP09 in MAM_CON/IMN than in
646 MAM_CON. J in PBL is very sensitive to the prefactor in WP09. Although the prediction of J
647 over ocean in PBL has been improved in MAM_CON/IMN, J over land areas in PBL is largely
648 underpredicted by factors of 1-100, resulting in degraded J performance in terms of globe mean.
649 The underprediction of J over land in PBL is likely due to the uncertainties in the nucleation
650 parameterizations (e.g., the missing species as mentioned previously). Large NMBs still remain
651 for COT, CWP, and CCN, indicating the uncertainties in the treatments of related atmospheric
652 processes such as cloud microphysics and aerosol-cloud interactions.
653
654 5.4 Impacts of Gas-Aerosol Partitioning
655 The inclusion of ISORROPIA II changes the mass concentrations of major $PM_{2.5}$ species
656 and their gaseous precursors. Changes in PM concentrations then affect predictions of cloud
657 variables and therefore radiation. Changes of radiation can also affect SO_2 oxidation by OH,
658 which affects H_2SO_4 concentrations. Figure 6 shows the absolute differences of H_2SO_4, fine
659 particulate sulfate (SO4f), NH_3, fine particulate ammonium (NH4f), HNO_3, fine particulate
660 nitrate (NO3f), HCl, and fine particulate chloride (CLf) for summer 2001 between MAM_CON

661 and MAM_CON/ISO. Similar plots for winter (December, January, and February (DJF)) 2001
662 are shown in Figure A1. Compared to MAM_CON, MAM_CON/ISO gives higher H_2SO_4
663 mixing ratios but lower SO4f concentrations. SWD increases with the global mean of 8.9 W m^{-2}
664 (~ 5.8%) in MAM_CON/ISO, which allows more production of OH from photolytic reactions of
665 VOCs, HONO, HNO_3, HNO_4, H_2O_2, HOCl, and HOBr, and therefore enhanced oxidation of SO_2
666 to form H_2SO_4. As shown in Figure 6, the mixing ratios of H_2SO_4 either increase up to 0.76 ppt
667 or decrease as large as 1.14 ppt, leading to a net increase of 0.002 ppt in terms of global mean.
668 The mass concentration of SO4f is mainly affected by H_2SO_4 condensation. Although the mixing
669 ratios of H_2SO_4 increase with the global mean change of 0.002 ppt, SO4f concentrations decrease
670 with the global mean of 0.02 μg m^{-3}, which are mainly due to less condensation of H_2SO_4 under
671 higher temperature conditions. In summer, the increase or decrease of H_2SO_4 can result in an
672 increase or a decrease of SO4f (e.g., over most oceanic areas). However, the decrease of SO4f
673 with the increase of H_2SO_4 over the India Ocean is mainly due to less H_2SO_4 condensation. For
674 the regions where SO4f increases over land, the increase of SO4f is due to more oxidation of SO_2
675 by OH. Compared to MAM_CON, the concentrations of NH_3, HNO_3, and HCl increase
676 significantly over most land areas, whereas NH4f, NO3f, and Clf decrease significantly over
677 most land areas in MAM_CON/ISO. Such changes can be explained based on the chemical
678 regimes and their spatial distributions as shown in Figure A2. Compared to MAM_CON, the
679 prediction of SWD in MAM_CON/ISO is improved with the NMB decreasing from -6.5% to -
680 2.2%. The predictions of involved species such as NH_4^+, NO_3^-, and Cl^- are improved
681 significantly by 13.6%~345.4%, although there is a slight degradation in the predictions of SO_4^{2-}
682 and O_3 over CONUS, CO, O_3, $PM_{2.5}$, and PM_{10} over Europe, PM_{10} over East Asia, and column
683 CO, NO_2, TOR, and J over globe. MAM_CON/ISO improves the predictions of HNO_3, NH_4^+,

684 NO_3^-, Cl^-, BC, OC, TC, and $PM_{2.5}$ over CONUS, SO_2, NH_3, NO_2, SO_4^{2-}, NH_4^+, NO_3^-, and Cl^-
685 over Europe, and CO and SO_2 over East Asia, which leads to improved performance in SWD,
686 column CCN5, and SWCF over globe, as shown in Table 3. As shown in Table A1, the changes
687 in most radiative and cloud variables between MAM_CON and MAM_CON/ISO are statistically
688 significant, indicating the significant impacts of ISORROIA II on the predictions of radiation,
689 aerosol, and cloud. ISORROPIA II calculates gas-aerosol partitioning under different
690 atmospheric conditions, significantly improving predictions of major gas precursor (e.g., HNO_3)
691 over CONUS and secondary aerosols (e.g., NO_3^- and Cl^-) over CONUS and Europe. Large
692 decreases in the concentrations of NO_3^- and Cl^- result in a decrease in NH_4^+, $PM_{2.5}$, and PM_{10},
693 thus decreasing CCN, CDNC, AOD, and the absolute value of SWCF.
694 MAM_CO/ISO assumes metastable conditions (i.e., assuming all salts in an aqueous
695 solution), which may introduce errors in gas/particle partitioning. The validity of this assumption
696 is examined by taking the absolute differences of the concentrations of major inorganic gas and
697 aerosol species between metastable (MAM_NEWA) and stable (MAM_NEWB) conditions (i.e.,
698 Figure A3). Compared with MAM_NEWA, the global average changes predicted by
699 MAM_NEWB are within 5% for most gaseous and aerosol species over non-desert/arid regions,
700 indicating that the assumption of metastable conditions is not a significant sources of uncertainty
701 in this work. However, the irreversible gas-to-particle mass transfer treatment for coarse
702 particles can potentially overpredict the concentrations of coarse particles (e.g., overpredictions
703 of Cl^- and NO_3^- over Europe).
704
705 5.5 Overall Impacts of All New and Modified Model Treatments

706 Compared to MAM_CB05_GE, the simulations with modified or new aerosol treatments
707 (MAM_CON, MAM_CON/IMN, MAM_CON/ISO, MAM_NEWA) slightly degrade the
708 prediction of LWD (increasing NMB from -0.9% to -1.4%), but improve the predictions of OLR,
709 CF, COT, and CWP slightly (with 0.6% - 10.4% decreases in their NMBs) and CDNC
710 significantly (reducing NMBs from -57.5% up to -13.4%). Although the CCN predictions are
711 somewhat degraded in MAM_CON and MAM_CON/IMN, they are improved significantly in
712 MAM_CON/ISO and MAM_NEWA (reducing NMBs from -61.6% to 1.8-6.3%). As shown in
713 Table A2, changes in most radiative and cloud variables between MAM_SIM and MAM_NEWA
714 are statistically significant, indicating the significant impacts of new and modified treatments on
715 predictions of radiation and cloud. Among all new and modified model treatments, the new gas-
716 phase chemistry simulates more gaseous species and improves the predictions of NH_3 over
717 Europe, $PM_{2.5}$ over CONUS and PM_{10} over East Asia. The modified condensation and aqueous-
718 phase chemistry simulate more aerosol species (NO_3^- and Cl^-) and improve the prediction of
719 HNO_3. MAM_CON also improves J in the PBL due to more available H_2SO_4 involving in the
720 homogeneous nucleation using an accommodation coefficient of 0.02 for H_2SO_4 condensation,
721 and improves the predictions of CDNC and AOD significantly. MAM_CON/IMN increases
722 PM_{num} above PBL and $PM_{2.5}$ and PM_{10} over Europe and improves the prediction of $PM_{2.5}$ over
723 CONUS and Europe. MAM_CON/ISO improves the predictions of HNO_3, NH_4^+, $PM_{2.5}$, NO_3^-,
724 and Cl^- over CONUS, NO_3^- and Cl^- over Europe, and CCN over globe, and improves the
725 predictions of SWCF most (with an NMB of 1.6%).
726 Large biases in some variables remain in MAM_NEWA due to uncertainties in model
727 inputs (e.g., meteorology and emissions) and model treatments (e.g., multi-phase chemistry, dust
728 emission scheme, cloud microphysics, aerosol activation, SOA formation, and dry and wet

729 deposition). The large NMBs of CO and SO_2 over East Asia, SO_2, NH_3, and NO_2 over Europe,
730 SO_2, and BC over CONUS are likely due to the uncertainties of emissions and the interpolation
731 of emissions from a fine-grid scale in the original emission inventories (e.g., county-based
732 emissions over CONUS) to a large-grid scale used in this work, which can result in large NMBs
733 in secondary aerosols (e.g., SO_4^{2-}, NH_4^+, NO_3^-, thus $PM_{2.5}$ and PM_{10}). Heterogeneous reactions
734 are not included in this work, which may help explain to some extent less oxidation and
735 underpredictions for PM species predictions (e.g., sulfate and nitrate) and overpredictions for
736 gaseous species. The large NMB of O_3 predictions over Europe in MAM_NEWA (with an NMB
737 of 62.7%) is mainly due to a lack of NO_x titration (as indicated by large underpredictions in NO_2)
738 and more production of O_3 from the photolytic reaction of NO_2 resulted from overpredictions of
739 SWD particularly in autumn and winter. Table 4 shows the seasonal statistics for O_3, NO_2, and
740 HNO_3 over Europe in MAM_NEWA. During autumn and winter, O_3 is overpredicted by about
741 100% ~ 140%, whereas NO_2 is underpredicted by about -85% ~ -20%, indicating insufficient
742 NO_x for titration of O_3 titration. SWD is overpredicted by 45.0 W m^{-2} (or by 58.4%), favoring the
743 photolytic reactions of NO_2 to produce O_3.Due to the uncertainties in the NO_x emissions, NO_2 is
744 underpredicted, causing less NO_2 to be oxidized to produce HNO_3, which results in an
745 underprediction of HNO_3 in winter. In autumn, SWD is overpredicted by 42.8 W m^{-2} (or by
746 37.9%). However, in autumn, although NO_2 is underpredicted due to the uncertainties in the NO_x
747 emissions, HNO_3 mixing ratios are overpredicted. SWD is stronger in autumn than in winter, and
748 mixing ratios of OH are higher due to photolytic reactions of overpredicted O_3 and additional
749 photolytic reactions of VOCs. Therefore, OH can oxidize NO_2 to produce HNO_3, resulting in the
750 overprediction of HNO_3. Simple aqueous-phase chemistry is included in this work, which could
751 result in high uncertainty in predicting aerosols in clouds. Decreased aerosol number

752 concentrations can result in a decrease of CCN and AOD directly. The underpredictions of
753 CDNC are likely due to uncertainties in the model treatments for aerosol activation and cloud
754 microphysics, which then result in large NMBs in COT and CWP. The large biases in OC and TC
755 indicate the uncertainties in the emissions of BC and primary OC, and the treatments for SOA
756 formation. The large NMB in particle formation rate J is likely due to uncertainties in model
757 inputs (e.g., SO_2 emissions) and model treatments (e.g., the accommodation coefficient of H_2SO_4
758 and missing participants in the current nucleation schemes).
759
760 5.6 Impacts of Adjusted Emissions
761 The evaluation and analyses of MAM_NEWA indicate that some large biases are caused
762 by inaccuracies in the emissions of CO, SO_2, BC, OC, and NH_3. The sensitivity simulation with
763 adjusted emissions of CO, SO_2, BC, OC, and NH_3 (MAM_NEW/EMIS) is performed to further
764 look into such impacts. For example, with 30% increase in CO emissions and 20% increase in
765 NH_3 emissions over Europe, the NMBs of surface concentrations of CO and NH_3 change from-
766 3.4% to 12.1%, -84.3% to -77.5%, respectively. On a global scale, the increased CO emissions
767 result in 3.0% absolute reduction in the NMB of column CO. The 30% reduction in SO_2
768 emissions and 20% increase in OC and BC emissions over CONUS result in 139.6%, 8.6%, and
769 24.9% absolute reduction in their NMBs. The 30% increase in CO emissions and 20% increase
770 in SO_2 over East Asia result in 3.3% and 7.8% absolute reduction in their NMBs.
771 As shown in Table 3, compared with MAM_NEWA, MAM_NEW/EMIS shows an
772 improved performance in the concentrations of SO_2, HNO_3, SO_4^{2-}, NH_3, and NH_4^+ over Europe,
773 SO_2, HNO_3, BC, OC, TC, NO_3^-, and Cl^- over CONUS, CO and SO_2 over Asia, and column CO
774 over globe. However, it degrades to some extent the performance of SO_4^{2-} and NH_4^+ over

775 CONUS, $PM_{2.5}$ and PM_{10} over Europe, PM_{10} over Asia, and J over globe. Decreased SO_2
776 emissions over CONUS result in a decrease of H_2SO_4 and therefore a decrease of SO_4^{2-}. Based
777 on aerosol thermodynamic treatments, decreased SO_4^{2-} will result in decreased NH_4^+. Therefore,
778 $PM_{2.5}$ and PM_{10} decrease as well. Adjusted emissions can affect secondary aerosol formations
779 and therefore radiative variables can be affected due to the direct and indirect effects of aerosols.
780 As shown in Table 2, compared with MAM_NEWA, MAM_NEW/EMIS reduces MB of LWD
781 by 9.3%, SWD by 37.5%, and CF by 18.9%, leading to 0.1% - 1.6% absolute reduction in their
782 NMBs. This illustrates the sensitivity of radiation to the perturbations in emissions through
783 chemistry feedbacks to the climate system. As shown in Table A1, only column CCN5 and AOD
784 are significantly different between MAM_NEWA and MAM_NEW/EMIS, indicating the
785 impacts of emissions are more significant on predictions of gas and aerosol than radiative
786 variables.
787
788 6. Evaluation of the Five-Year Simulations
789 6.1. Performance Evaluation
790 Tables 5 and 6 show the statistical performance for radiative/cloud variables and
791 chemical predictions, respectively, from the 5-yr simulations using three different configurations.
792 Compared with MAM_SIM_5Y, MAM_NEW_5YA improves the predictions of aerosol and
793 cloud variables such as AOD, COT, CWP, CCN5, and CDNC (with 4.8% to 23.4% absolute
794 reduction in their NMBs), and radiative variables such as SWD, LWD, OLR, and SWCF (with
795 0.4-4.2% absolute reduction in their NMBs). MAM_NEW_5YA also shows slight improvement
796 for the predictions of SO_4^{2-} and BC over CONUS and SO_2 over East Asia (with 0.3-2.3%
797 absolute reduction in their NMBs), but moderate-to-large improvements for the predictions of

798 OC, TC, and $PM_{2.5}$ over CONUS, PM_{10} over East Asia, and SO_2, $PM_{2.5}$, and PM_{10} over Europe
799 (with 5.2-20.1% absolute reduction in their NMBs). Compared to TOR calculated based on O_3
800 climatology used in MAM_SIM_5Y, TOR predicted from MAM_NEW_5YA is slightly
801 improved with 1.2%, 1.3%, and 0.3 absolute reduction in its NMB, NME, and RMSE,
802 respectively. Evaluation of major radiative/cloud variables and chemical predictions are also
803 conducted for June, July, and August (JJA) of 2001-2005, which is shown in Tables A3 and A4
804 in the supplementary material. Compared with full 5-year (2001-2005) average, the simulation
805 for JJA gives similar predictions for chemical species but better model predictions for radiation
806 (e.g., LWD, SWD, and OLR) and cloud (e.g., COT, CWP, column CCN5, and CDNC) variables.
807 Tables 5 and 6 also show the performance of MAM_NEW_5YB in which CAM5 is fully
808 coupled with land, ocean, and ice models. The performance is overall similar for all radiative
809 variables and most chemical species between MAM_NEW_5YA and MAM_NEW_5YB (most
810 within 5% differences in the absolute values of their NMBs). The performance of HNO_3 over
811 CONUS and Europe, NH_4^+, NO_3^-, and Cl^- over Europe, PM_{10} over Europe and East Asia is
812 improved appreciably (with 4.2-17.9% reduction in the absolute values of their NMBs), and that
813 of SO_2 over CONUS and Europe and NH_4^+, NO_3^-, and Cl^- over CONUS degrades appreciably
814 (with 4.3-8.5% increase in the absolute values of their NMBs). Those changes are mainly due to
815 the interactions among Earth's components, particularly at the interface of earth components
816 (e.g., air-sea, air-land, and sea-ice interfaces) and feedbacks to the climate system, which in turn
817 affects gaseous and aerosol concentrations in the coupled system.
818 Large biases remain for some variables in MAM_NEW_5YA and MAM_NEW_5YB due
819 to uncertainties in model inputs (e.g., meteorology and emissions) and model treatments (e.g.,
820 multi-phase chemistry, dust emission scheme, cloud microphysics, aerosol activation, SOA

formation, and dry and wet deposition), which have been illustrated in Section 5.5. Large biases in Cl^- predictions over Europe are likely due to the combined effects of a low concentration of observed Cl^-, uncertainties in HCl emissions, and inaccurate predictions of coarse Cl^- in the model since ISORROPIA II is only implemented for fine particles. Uncertainties in the mass accommodation coefficients of volatile gas species can also result in uncertainties in predictions of condensable gases.

6.2 Impact of New and Modified Treatments on 5-year (2001-2005) Simulations

Figure 7 shows the absolute differences of surface SO_2, NH_3, SO_4^{2-}, NH_4^+, TC, $PM_{2.5}$, PM_{10}, J, and aerosol number (PM_{num}) and Figure 8 shows the absolute differences of radiative variables between MAM_SIM_5Y and MAM_NEW_5YA. The new and modified model treatments in MAM_NEW_5YA cause changes in the concentrations of PM and precursor gases, which affect radiative variables through aerosol direct and indirect effects. The changes in radiative variables in turn affect gas-phase chemistry and aerosol processes. As shown in Figure 7, the difference of SO_2 between the two simulations varies from -1.7 to 3.8 ppb, with a global mean difference of 4.2 ppt. The decrease of SO_2 over most oceanic area is mainly due to the decrease of DMS resulted from less oxidation by OH radicals. The increase of SO_4^{2-} over East Asia and eastern U.S. drives more NH_3 from gas-phase to particulate phase to form NH_4^+ through thermodynamic equilibrium, increasing the concentrations of NH_4^+ over these regions. However, the concentrations of SO_4^{2-} decrease over Europe due in part to less oxidation of SO_2. Despite such a decrease, the concentrations of NH_4^+ are higher over Europe due to the neutralization of NH_3 by Cl^- and NO_3^- that are treated in MAM_NEW_5YA but not treated in in MAM_SIM_5Y. Compared with MAM_SIM_5Y, J from MAM_NEW_5YA increases over

844 globe with a global mean difference of 0.066 cm^{-3} s^{-1}, due to the use of a lower mass
845 accommodation coefficient of H_2SO_4 in MAM_NEW_5YA, resulting in more available H_2SO_4
846 vapor participating in nucleation. The increases in J result in an increase in aerosol mass and
847 number concentrations and thus higher concentrations of $PM_{2.5}$ and PM_{10} (which improve
848 appreciably their performance, see Table 5).
849 As shown in Figure 8, compared with MAM_SIM_5Y, AOD increases by 0.007, column
850 CCN5 increases by 3.8×10^7 cm^{-2}, and CDNC increases by 16.1 cm^{-3} in MAM_NEW_5YA.
851 Higher PM_{num} in MAM_NEW_5YA allows more aerosol to grow into the CCN size, leading to
852 higher CCN in MAM_NEW_5YA. Higher aerosol concentrations in MAM_NEW_5YA result in
853 higher AOD. The increased aerosol number and mass concentration result in an increase in the
854 predictions of cloud variables through the aerosol-cloud interactions. For example, with all the
855 modified and new treatments, COT increases by 0.8, CWP increases by 4.1 g m^{-2}, and PWV
856 increases by 0.026 cm on global average. Due to the aerosol direct and indirect effects, the
857 difference in simulated SWD varies from -19.3.0 to 10.4 W m^{-2} and decreases by 3.4 W m^{-2} (~
858 2.0%) on a global average. The difference in LWD varies from -4.2 to 8.5 W m^{-2} and increases by
859 1.0 W m^{-2} (~ 0.4%) on a global average (Figure not shown). The difference in SWCF varies from
860 -8.4 to 17.9 W $m^{-2,}$ with a net increase of 2.7 W m^{-2} (~ 6.4%) on a global average. The absolute
861 differences of surface chemical species and major cloud/radiative variables for JJA average of
862 2001-2005 are shown in Figures A4 and A5 in the supplementary material. Compared with 5-
863 year average, the absolute changes of most radiative variables are smaller in JJA. The absolute
864 changes of PM_{10} are smaller in JJA, which is mainly due to the dust events during other months
865 (e.g., March-May over East Asia).
866

867 6.3 Global Burden Analysis

868 Table 7 shows the simulated global burdens of major gas and aerosol species for 2001-
869 2005. The global burdens of most gaseous precursors of aerosol are higher in MAM_NEW_5YA
870 than MAM_SIM_5Y (except for NH_3), due mainly to the incorporation of ISORROPIA II in
871 MAM_NEW_5YA. The global burden of tropospheric O_3 is higher in MAM_NEW_5YA than
872 MAM_SIM_5Y, which is due to higher mixing ratios of O_3 precursors (e.g., NO_2 and VOCs) that
873 are simulated in MAM_NEW_5YA. The global burdens of most gas species are comparable with
874 previous studies (Horowitz et al.2006; Lamarque et al., 2006; Williams et al., 2009; Liu et al.,
875 2012) with absolute differences of less than 20%. One exception is H_2SO_4, which is higher by a
876 factor 5 in MAM_NEW_5YA than in MAM_SIM_5Y. The higher burden of H_2SO_4 in
877 MAM_NEW_5YA is likely due to the less condensation of H_2SO_4 resulted from the use of a
878 lower mass accommodation coefficient. SO_4^{2-} burden is higher by 8.3% in MAM_NEW_5YA
879 than MAM_SIM_5Y, which is likely due to greater SO_2 oxidation in MAM_NEW_5YA. Higher
880 SO_4^{2-} burden results from higher SO_2 burden. Higher SO_2 burden leads to more SO_2 to be
881 oxidized to produce SO_4^{2-}, which overweighs the impacts from less H_2SO_4 condensation due to
882 lower mass accommodation coefficient. More SO_4^{2-} result in more NH_4^+. The burdens of BC and
883 POM are lower by 16.5% and 23.8%, respectively, in MAM_NEW_5YA than in MAM_SIM_5Y,
884 which is likely due in part to greater dry deposition fluxes and in part to a slower primary carbon
885 aging rate resulted from reduced condensation of gas species in MAM_NEW_5YA.
886 Condensation onto the primary carbon mode produces aging of the particles in this mode. A
887 lower accommodation coefficient is used in MAM_NEW_5YA, which results in less
888 condensation. Therefore, the fraction of aged particles has decreased. The global burdens of most
889 aerosol species are in the range of previous studies. For example, global burdens of SO_4^{2-} and

890 NH_4^+ from MAM_SIM_5Y and MAM_NEW_5YA are 23.4% and 17.0%, respectively, and
891 16.7% and 12.5%, respectively, lower than Liu et al. (2012), which is likely because
892 MAM_SIM_5Y contains no SO_4^{2-} emissions but Liu et al. (2012) included additional SO_4^{2-}
893 emissions of 1.66 Tg S yr^{-1}. Higher SO_4^{2-} emission leads to more SO_4^{2-} concentrations thus more
894 NH_4^+ in Liu et al. (2012). Compared with Horowitz et al. (2006), global burdens of BC and OC
895 from MAM_NEW_5YA are lower by 72.9% and 52.3%, respectively. Compared with Liu et al.
896 (2012), MAM_NEW_5YA gives comparable BC and POM burdens but much lower SOA (by a
897 factor of 3.0). Compared with Textor et al. (2006), POM burden is a factor of 3.5 lower in
898 MAM_NEW_5YA. The lower BC, OC, POM, and SOA burdens are likely due to the
899 uncertainties in the BC and OC emissions used as well as differences in the model treatments for
900 SOA formation and POM aging.

901

902 **7. Conclusions and Future work**

903 In this work, a new gas-phase chemistry mechanism and several advanced inorganic
904 aerosol treatments have been incorporated into CESM/CAM5.1-MAM7. These include (1) the
905 CB05_GE gas-phase chemical mechanism coupled with MAM7; (2) the condensation and
906 aqueous-phase chemistry involving HNO_3/ NO_3^- and HCl/ Cl^-; (3) an ion-mediated nucleation
907 (IMN) parameterization for the new particle formation from ions, (4) an inorganic
908 thermodynamic module, ISORROPIA II, that explicitly simulates thermodynamics of SO_4^{2-},
909 NH_4^+, NO_3^-, Cl^-, and Na^+ as well as the impact of crustal species, such as Ca^{2+}, K^+, and Mg^{2+}, on
910 aerosol thermodynamics. CB05_GE with new and modified inorganic aerosol treatments in
911 MAM7 simulates 139 species with 273 chemical reactions, which is more accurate than simple
912 gas chemistry coupled with default MAM7. Seven 1-yr simulations for 2001 and three 5-yr

913 simulations for 2001-2005 with different model configurations are performed to evaluate the
914 capabilities of the original and improved CESM/CAM5 and the mechanisms underlying
915 differences among model predictions.

916 Comparing to the simple gas-phase chemistry, the 2001 simulation with CB05_GE can
917 predict many more gaseous species, and give improved performance for predictions of organic
918 carbon and $PM_{2.5}$ over CONUS, NH_3 and SO_4^{2-} over Europe, SO_2 and PM_{10} over East Asia, and
919 cloud properties such as CF, CDNC, and SWCF. MAM_CON simulates NO_3^- and Cl^-, which are
920 important inorganic aerosols. With species-dependent accommodation coefficients for gas
921 condensation, more H_2SO_4 can participate in homogeneous nucleation, resulting in the
922 improvement of predictions of $PM_{2.5}$, PM_{10}, J, CDNC, and SWCF. IMN can increase the
923 predictions of J and PM_{num} in the upper atmosphere and thus improve the predictions of AOD,
924 CCN, and cloud properties, and SWCF over globe, $PM_{2.5}$ over CONUS and Europe, PM_{10} over
925 Europe and East Asia, and PM composition over Europe. The 2001 simulation with ISORROPIA
926 II can improve the predictions of major gas and aerosol species significantly, including HNO_3,
927 NH_4^+, NO_3^-, Cl^-, BC, OC, TC, and $PM_{2.5}$ over CONUS, SO_2, NH_3, NO_2, SO_4^{2-}, NH_4^+, NO_3^-, and
928 Cl^- over Europe, and CO and SO_2 over East Asia. Such improvements lead to improved
929 predictions of SWD, SWCF, and CCN5 over globe. The 2001 simulation with the new and
930 modified inorganic aerosol treatments appreciably improve the predictions of OLR, CF, COT,
931 CWP, PWV, CCN, CDNC, SWCF, J over globe, and HNO_3, NH_4^+ (CONUS), $PM_{2.5}$, and PM_{10}.
932 The 2001 sensitivity simulation with adjusted emissions further improves model predictions of
933 CO and SO_2 over East Asia, SO_2, HNO_3, NO_3^-, Cl^-, BC, OC, and TC over CONUS, SO_2, NH_3,
934 NH_4^+, HNO_3, NO_3^-, and Cl^- over Europe, and column CO and SWD over globe. The change of
935 emissions can affect primary gaseous precursors directly, and secondary gaseous species

936 indirectly through gas-phase chemistry. Meanwhile, secondary aerosols can be affected by
937 gaseous precursors, and therefore have impacts on cloud properties as well as direct and indirect
938 effects on radiation. Reducing the uncertainty of emissions can thus help reduce the model biases
939 significantly.

940 The comparison of the 5-yr simulations with prescribed SST shows that
941 MAM_NEW_5YA with CB05_GE can appreciably improve the predictions of AOD, COT, CWP,
942 CCN5, CDNC, SWD, LWD, OLR, and SWCF on global scale and OC, TC, and $PM_{2.5}$ over
943 CONUS, PM_{10} over East Asia, and SO_2, $PM_{2.5}$, and PM_{10} over Europe. The performance is
944 overall similar for all radiative variables and most chemical species between MAM_NEW_5YA
945 with prescribed SST and MAM_NEW_5YB in a fully-coupled mode.

946 In addition to uncertainties in emissions, additional uncertainties exist in the model
947 treatments. For example, the large biases in the predictions of O_3 over Europe and East Asia are
948 mainly due to insufficient NO_x titration resulting from the uncertainties in the NO_x emissions.
949 The large biases in PM_{10} over East Asia and Europe may be mainly due to the inaccurate
950 predictions of dust. The large bias in Cl^- over Europe may be due to the inaccurate predictions of
951 HCl and coarse Cl^-, resulted from the irreversible condensation of HCl over coarse mode
952 particles, and the uncertainty in the mass accommodation coefficient of HCl used. A reversible
953 condensation treatment should be used for volatile species in the future, which can more
954 accurately simulate the gas/particle partitioning of those volatile species over coarse mode
955 particles. Assumptions associated with equilibrium partitioning for fine particles such as
956 metastable conditions may be responsible for biases over desert/arid regions under low RH
957 conditions. In the default and modified nucleation treatments, it only considers H_2SO_4, NH_3,
958 H_2O, and ions involving in the new particle formation. Missing species (e.g., organics, iodine

compounds, and DMS) may also contribute to the new particle formation. Uncertainties in treating organic gas-aerosol partitioning may contribute to the inaccurate predictions of SOA, OC, TC, and PM. The large biases in CDNC, COT, and LWP indicate the uncertainties in cloud microphysics schemes and aerosol-cloud interaction parameterizations, which also limit the ability of climate and Earth system models to quantify aerosol indirect effects (Stephens, 2005; Gettelman et al., 2008). In addition to uncertainties in the model treatments, uncertainties in the model simulation settings such as the use of a coarse grid resolution and a large model time step of 1800 seconds for solving the chemical system in this work may contribute to the model biases. The representations of some of the aforementioned uncertain processes in CESM/CAM5.1 are being further improved by the authors' group. Decadal simulations using improved CESM/CAM5.1 will be conducted in the future to study the interactions among atmospheric chemistry, aerosol, and climate change and reduce associated uncertainties.

Acknowledgments

This work is sponsored by the U.S. NSF EaSM program AGS-1049200. The authors would like to thank Fangqun Yu for providing the IMN scheme, Athanasios Nenes for providing ISORROPIA II, Xiaohong Liu for providing a version of MAM7 that works in CAM5.0 and CAM5.1, Ralf Bennartz and John Rausch for providing CDNC data, Steve J. Ghan and Richard C. Easter for insightful discussions, and Shuai Zhu, a former postdoc researcher of the air quality forecasting laboratory at NCSU for early work on the incorporation of CB05_GE and its coupling with MAM3. The authors would also like to thank the four reviewers for their valuable suggestions that help improve the technical quality of this work. MODIS data and CERES data are provided by NASA via http://ladsweb.nascom.nasa.gov and

http://ceres.larc.nasa.gov/order_data.php, respectively. Other surface network data were downloaded from their respective web sites. We would like to acknowledge high-performance computing support from Yellowstone (ark:/85065/d7wd3xhc) provided by NCAR's Computational and Information Systems Laboratory, sponsored by the U.S. National Science Foundation.

References

Abdul-Razzak, H. and Ghan, S. J.: A Parameterization of Aerosol Activation, Part 2: Multiple Aerosol Types, J. Geophys. Res., 105, 6837-6844, 2000.

Adams, P. J. and Seinfeld, J. H.: Predicting global aerosol size distributions in general circulation models, J. Geophys. Res., 107(D19), 4370, doi:10.1029/2001JD001010, 2002.

Appel, K.W., Pouliot, G. A., Simon, H., Sarwar, G., Pye, H. O. T., Napelenok, S. L., Akhtar, F., and Roselle, S. J.: Evaluation of dust and trace metal estimates from the Community Multiscale Air Quality (CMAQ) model version 5.0, Geosci. Model Dev., 6, 883-899, 2013.

Arstila, H., Korhonen, P., and Kulmala, M.: Ternary nucleation: Kinetics and application to water-ammonia-hydrochloric acid system, J. Aerosol Sci., 30, 131-138, doi:10.1016/S0021-8502(98)00033-0, 1999.

Barth, M. C., Rasch, P. J., Kiehl, J. T., Benkovitz, C. M., and Schwartz, S. E.: Sulfur chemistry in the National Center for Atmospheric Research Community Climate Model: Description, evaluation, features and sensitivity to aqueous chemistry, J. Geophys. Res., 105, 1387-1415, 2000.

Berndt, T., Sipilä, M., Stratmann, F., Petäjä, T., Vanhanen, J., Mikkilä, J., Patokoski, J., Taipale, R., Lee Mauldin III, R., and Kulmala, M.: Enhancement of atmospheric H_2SO_4/H_2O nucleation: organic oxidation products versus amines, Atmos. Chem. Phys. Discuss., 13, 16301-16335, doi:10.5194/acpd-13-16301-2013, 2013.

Bennartz, R.: Global assessment of marine boundary layer cloud droplet number concentration from satellite, J. Geophys. Res., 112, D02201, doi: 10.1029/2006JD007547, 2007.

Bey, I., Jacob, D. J., Yantosca, R. M., Logan, J. A., Field, B. D., Fiore, A. M., Li, Q., Lui, H. Y., Mickley, L. J., and Schultz, M. G.: Global modeling of tropospheric chemistry with assimilated meteorology: Model description and evaluation, J. Geophys. Res., 106(D19), 23073-23095, 2001.

Bretherton, C. S. and Park, S.: A new moist turbulence parameterization in the community atmosphere model, J. Climate, 22, 3422-3448, 2009.

1015 Byun, D. W. and Schere, K. L.: Review of the governing equations, computational algorithms,
1016 and other components of the Models-3 Community Multiscale Air Quality (CMAQ)
1017 Modeling System, Appl. Mech. Rev., 59, 51-77, 2006.

1018 Capaldo, K. P., C. Pilinis, and S. N. Pandis: A computationally efficient hybrid approach for
1019 dynamic gas/aerosol transfer in air quality models, Atmos. Environ., 34, 3617– 3627, 2000.
1020
1021 Collins, W. D., Bitz, C. M., Blackmon, M. L., Bonan, G. B., Bretherton, C. S., Carton, J. A.,
1022 Chang, P., Doney, S. C., Hack, J. J., Henderson, T. B., Kiehl, J. T., Large, W. G., McKenna, D.
1023 S., Santer, B. D., and Smith, R. D.: The Community Climate System Model version3
1024 (CCSM3), J. Clim., 19, 2122-2143, doi:10.1175/JCLI3761.1, 2006.

1025 Dunne, J. P., John, J. G., Adcroft, A. J., Griffies, S. M., Hallberg, R. W., Shevliakova, E.,
1026 Stouffer, R. J., Cooke, W., Dunne, K. A., Harrison, M. J., Krasting, J. P., Malyshev, S. L.,
1027 Milly, P. C. D., Phillipps, P. J., Sentman, L. T., Samuels, B. L., Spelman, M. J., Winton, M.,
1028 Wittenberg, A. T., and Zadeh, N.: GFDL's ESM2 global coupled climate-carbon earth system
1029 models. Part I: Physical formulation and baseline simulation characteristics, J. Climate, 25,
1030 6646-6665, 2012.

1031 Dutkiewicz, S., Sokolov, A. P., Scott, J., and Stone, P. H.: A Three-Dimensional Ocean-Seaice-
1032 Carbon Cycle Model and its Coupling to a Two-Dimensional Atmospheric Model: Uses in
1033 Climate Change Studies. MIT JPSPGC Report 122, May, 47 p, 2005.

1034 Emmons, L. K., Walters, S., Hess, P. G., Lamarque, J.-F., Pfister, G. G., Fillmore, D., Granier, C.,
1035 Guenther, A., Kinnison, D., Laepple, T., Orlando, J., Tie, X., Tyndall, G., Wiedinmyer, C.,
1036 Baughcum, S. L., and Kloster, S.: Description and evaluation of the Model for Ozone and
1037 Related chemical Tracers, version 4 (MOZART-4), Geosci. Model Dev., 3, 43-67,
1038 doi:10.5194/gmd-3-43-2010, 2010.

1039 ENVIRON: Comprehensive Air Quality Model with extensions User's Guide, Novato,
1040 California, USA, 5.3 edn., 2010.

1041 Faraji, M., Kimura, Y., McDonald-Buller, E., and Allen, D.: Comparison of the carbon bond and
1042 SAPRC photochemical mechanisms under conditions relevant to southeast Texas, Atmos.
1043 Environ., 42, 5821–5836, doi:10.1016/j.atmosenv.2007.07.048, 2008.

1044 Fast, J. D., Gustafson Jr., W. I., Easter, R. C., Zaveri, R. A., Barnard, J. C., Chapman, E. G.,
1045 Grell, G. A., and Peckham, S. E.: Evolution of ozone, particulates, and aerosol direct radiative
1046 forcing in the vicinity of Houston using a fully coupled meteorology-chemistry-aerosol
1047 model, J. Geophys. Res., 111, D21305, doi:10.1029/2005JD006721, 2006.

1048 Fountoukis, C and Nenes, A.: ISORROPIA II: a computationally efficient thermodynamic
1049 equilibrium model for K^+- Ca^{2+} -Mg^{2+} -NH_4^+ -Na^+-SO_4^{2-}-NO_3^--Cl^--H_2O aerosols, Atmos.
1050 Chem. Phys., 7, 4639–4659, doi:10.5194/acp-7-4639-2007, 2007.

1051 Gettelman, A., Morrison, H., and Ghan, S. J.: A new two-moment bulk stratiform cloud
1052 microphysics scheme in the community atmosphere model, version 3 (CAM3). Part II:
1053 Single-column and global results, J. Climate, 21(15), 3660-3679, 2008.

1054 Ghan, S. J., and Zaveri, R. A.: Parameterization of optical properties for hydrated internally
1055 mixed aerosol, J. Geophys. Res., 112, D10201, doi:10.1029/2006JD007927,2007.

1056 Ghan, S. J., Liu, X., Easter, R. C., Zaveri, R., Rasch, P. J., and Yoon, J.-H.: Toward a minimal
1057 representation of aerosols in climate models: comparative decomposition of aerosol direct,
1058 semidirect, and indirect radiative forcing, J. Climate, 25, 6461-6476, 2012.

1059 Guenther A., Karl, T., Harley, P., Wiedinmyer, C., Palmer, P. I., and Geron, C.: Estimates of
1060 global terrestrial isoprene emissions using MEGAN (Model of Emissions of Gases and
1061 Aerosols from Nature), Atmos. Chem. Phys., 6, 3181-3210, 2006.

1062 Heald, C. L., Henze, D. K., Horowitz, L. W., Feddema, J., Lamarque, J.-F., Guenther, A., Hess, P.
1063 G., Vitt, F., Seinfeld, J. H., Goldstein, A. H., and Fung, I.: Predicted change in global
1064 secondary organic aerosol concentrations in response to future climate, emissions, and land
1065 use change, J. Geophys. Res., 113, D05211, doi:10.1029/2007JD009092, 2008.

1066 Heintzenberg, J.: Fine particles in the global troposphere, A review. Tellus, 41B, 149-160, 1989.

1067 Hoffmann, T., O'Dowd, C. D., and Seinfeld, J. H.: Iodine oxide homogeneous nucleation: An
1068 explanation for coastal new particle production, Geophys. Res. Lett., 28(10), 1949-1952,
1069 2001.

1070 Horowitz, L. W.: Past, present, and future concentrations of tropospheric ozone and aerosols:
1071 methodology, ozone evaluation, and sensitivity to aerosol wet removal, J. Geophys. Res., 111,
1072 D22211, doi:10.1029/2005JD006937, 2006.

1073 Hu, X.-M., Y. Zhang, M. Z. Jacobson, and C. K. Chan: Coupling and evaluating gas/particle mass
1074 transfer treatments for aerosol simulation and forecast, J. Geophys. Res., 113, D11208,
1075 doi:10.1029/2007JD009588, 2008.

1076 Iacono, M. J., Delamere, J. S., Mlawer, E. J., and Clough, S. A.: Evaluation of upper tropospheric
1077 water vapor in the NCAR Community Climate Model (CCM3) using modeled and observed
1078 HIRS radiances, J. Geophys. Res., 108(D2), 4037, doi:10.1029/2002jd002539, 2003.

1079 Iacono, M. J., Delamere, J. S., Mlawer, E. J., Shephard, M. W., Clough S. A., and Collins, W. D.:
1080 Radiative forcing by long-lived greenhouse gases: Calculations with the AER radiative
1081 transfer models, J. Geophys. Res., 113(D13), D13103, doi:10.1029/2008jd009944, 2008.

1082 Jacobson, M. Z.: Studying the effect of calcium and magnesium on size-distributed nitrate and
1083 ammonium with EQUISOLV II, Atmos. Environ., 33, 3635-3649, 1999.

1084 Jacobson, M. Z.: Short-term effects of Controlling Fossil-Fuel Soot, Biofuel Soot and Gases, and
1085 Methane on Climate , Arctic Ice, and Air Pollution Health, J. Geophys. Res., 115, D14209,
1086 doi:10.1029/2009JD013795, 2010.

1087 Jacobson, M. Z. (2005), A solution to the problem of nonequilibrium acid/base gas-particle transfer at
1088 long time step, Aerosol Sci. Technol., 39, 92– 103.

1089 Karamchandani, P., Zhang, Y., Chen, S.-Y., and Balmori-Bronson, R.: Development of an
1090 extended chemical mechanism for global-through-urban applications, Atmospheric Pollution
1091 Research, 3, 1-24, 2012.

1092 Kelly, J. T., P. V. Bhave, C. G. Nolte, U. Shankar, and K. M. Foley: Simulating emission and
1093 chemical evolution of coarse sea-salt particles in the Community Multiscale Air Quality
1094 (CMAQ) model, Geosci. Model Dev., 3, 257–273, 2010.

1095 Kim, Y., Sartelet, K., and Seigneur, C.: Formation of secondary aerosols: impact of the gas-phase
1096 chemical mechanism, Atmos. Chem. Phys., 11, 583-598, doi:10.5194/acp-11-583-2011,
1097 2011a.

1098 Koloutsou-Vakakis S., Rood, M. J., Nenes, A., and Pilinis, C.: Modeling of aerosol properties
1099 related to direct climate forcing, J. Geophys. Res., 103(D14), 17009-17032, doi:
1100 10.1029/98JD00068, 1998.

1101 Kulmala, M., Vehkamaki, H., Petaja, T., Dal Maso, M., Lauri, A., Kerminen, V.-M., Birmili, W.,
1102 and McMurry, P.: Formation and growth rates of ultrafine atmospheric particles: A review of
1103 observations, J. Aerosol Sci., 35, 143-176, 2004.

1104 Lamarque, J.-F., Kiehl, J. T., Hess, P. G., Collins, W. D., Emmons, L. K., Ginoux, P., Luo, C., and
1105 Tie, X. X.: Response of a coupled chemistry-climate model to changes in aerosol emissions:
1106 global impact on the hydrological cycle and the tropospheric burdens of OH, ozone, and NOx,
1107 J. Geophys. Res., 32, L16809, doi:10.1029/2005GL023419, 2005.

1108 Lamarque, J. F., Emmons, L. K., Hess, P. G., Kinnison, D. E., Tilmes, S., Vitt, F., Heald, C. L.,
1109 Holland, E. A., Lauritzen, P. H., Neu, J., Orlando, J. J., Rasch, P. J., and Tyndall, G. K.:CAM-
1110 chem: description and evaluation of interactive atmospheric chemistry in CESM, Geosci.
1111 Model Dev., 5, 369-411, doi:10.5194/gmd-5-369-2012, 2012.

1112 Lawrence, D. M., Oleson, K. W., Flanner, M. G., Thornton, P. E., Swenson, S. C., Lawrence, P.
1113 J., Zeng, X., Yang, Z.-L., Levis, S., Sakaguchi, K., Bonan, G. B., and Slater, A. G.:
1114 Parameterization improvements and functional and structural advances in version 4 of the
1115 Community Land Model, J. Adv. Model. Earth Syst., 3, Art. 2011MS000045, 27 pp, doi:
1116 10.1029/2011MS000045, 2011.

1117 Liao, H., Adams, P. J., Chung, S. H., Seinfeld, J. H., Mickley, L. J., and Jacob, D. J.: Interactions
1118 between tropospheric chemistry and aerosols in a unified general circulation model, J.
1119 Geophys. Res., 108(D1), 4001, doi:10.1029/2001JD001260, 2003.

1120 Liu, X., Easter, R. C., Ghan, S. J., Zaveri, R., Rasch, P., Shi, X., Lamarque, J.-F., Gettleman, A.,
1121 Morrison, H., Vitt, F., Conley, A., Park, S., Neale, R., Hannay, C., Ekman, A. M. L., Hess, P.,
1122 Mahowald, N., Collins, W., Iacono, M.J., Bretherton, C. S., Flanner, M. G., and Mitchell,
1123 D.L.: Toward a minimal representation of aerosols in climate models: description and
1124 evaluation in the Community Atmosphere Model CAM5, Geosci. Model Dev., 5, 709-739,
1125 2012.

1126 Marsh, A. R. W., and McElory, W. J.: The dissociation constant and Henry's law constant of HCl
1127 in aqueous solution, Atmos. Environ., 19, 1075-1080, 1985.

1128 Martensson, E. M., Nilsson, E. D., deLeeuw, G., Cohen, L. H., and Hansson, H. C.: Laboratory
1129 simulations and parameterization of the primary marine aerosol production, J. Geophys. Res.,
1130 108(D9), 4297, doi:10.1029/2002JD002263, 2003.

1131 Meng, Z. and Seinfeld, J. H.: Time scales to achieve atmospheric gas-aerosol equilibrium for
1132 volatile species, Atmos. Environ., 30, 2889-2900, 1996.

1133 Meng, Z, Dabdub, D., and Seinfeld, J.H.: Size- and chemically-resolved model of atmospheric
1134 aerosol dynamics. J. Geophys. Res., 103, 3419-3435, 1998.

1135 Merikanto, J., Napari, I., Vehkamaki, H., Anttila, T., and Kulmala, M.: New parameterization of
1136 sulfuric acid-ammonia-water ternary nucleation rates at tropospheric conditions, J. Geophys.
1137 Res., 112, D15207, doi: 10.1029/2006JD007977, 2007.

1138 Morrison, H. and Gettelman, A.: A new two-moment bulk stratiform cloud microphysics scheme
1139 in the community atmosphere model, version 3 (CAM3). Part I: Description and numerical
1140 tests, J. Climate, 21(15), 3642-3659, 2008.

1141 Nenes, A., Pandis, S.N., and Pilinis, C.: ISORROPIA: A new thermodynamic equilibrium model
1142 for multiphase multicomponent inorganic aerosols, Aquatic Geochemistry, 4, 123-152, 1998.

1143 Olerud, D. and Sims, A. (2004). MM5 2002 Modeling in Support of VISTAS (Visibility
1144 Improvement – State and Tribal Association of the Southeast), Report, Baron Advanced
1145 Meteorological Systems, LLC, Raleigh, NC, August.

1146 Park, S. and Bretherton, C. S.: The university of Washington shallow convection and moist
1147 turbulence schemes and their impact on climate simulations with the community atmosphere
1148 model, J. Climate, 22, 3449-3469, 2009.

1149 Raes, F., Augustin, J., and Vandingenen, R.: The role of ion-induced aerosol formation in the
1150 lower atmosphere, J. Aerosol Sci., 17, 466-470, doi: 10.1016/0021-8502(86)90135-7, 1986.

1151 Reiter, R.: Phenomena in atmospheric and environmental electricity, Elsevier, New York, 1992.

1152 Sander S. P., Friedl, R. R., Golden, D. M., Kurylo, M. J., Huie, R. E., Orkin, V. L., Moortgat, G.
1153 K., Ravishankara, A. R., Kolb, C. E., Molina, M. J., and Finlayson-Pitts, B. J.: Chemical
1154 Kinetics and Photochemical Data for Use in Atmospheric Studies, National Aeronautics and
1155 Space Administration, Jet Propulsion Laboratory California Institute of Technology Pasadena,
1156 California, 2003.

1157 Seinfeld, J. H. and Pandis, S. N.: Atmospheric chemistry and physics: From air pollution to
1158 climate change, 2 ed., John Wiley & Sons, Inc, 2006.

1159 Sihto, S. L., Kulmala, M., Kerminen, V. M., Maso, M. D., Petaja, T., Riipinen, I., Korhonen, H.,
1160 Arnold, F., Janson, R., Boy, M., Laaksonen, A., and Lehtinen, K. E. J.: Atmospheric sulphuric
1161 acid and aerosol formation: implications from atmospheric measurements for nucleation and
1162 early growth mechanisms, Atmospheric Chemistry and Physics, 6, 4079-4091, 2006.

1163 Sokolov, A. P., Schlosser, C. A., Dutkiewicz, S., Paltsev, S., Kicklighter, D., Jacoby, H. D., Prinn,
1164 R. G., Forest, C. E., Reilly, J. M., Wang, C., Felzer, B., Sarofim, M. C., Scott, J., Stone, P. H.,

Melillo, J. M., and Cohen, J.: The MIT Integrated Global System Model (IGSM) Version 2: Model Description and Baseline Evaluation. MIT JPSPGC Report 124, July, 40 p, 2005.

Spracklen, D. V., Carslaw, K. S., Kulmala, M., Kerminen, V.-M., Mann, G. W., and Sihto, S.-L.: The contribution of boundary layer nucleation events to total particle concentrations on regional and global scales, Atmos. Chem. Phys., 6, 5631-5648, 2006.

Stephens, G. L.: Cloud feedbacks in the climate system: A critical review, J. Climate, 18(2), 237-273, 2005.

Stier, P., Feichter, J., Kinne, S., Kloster, S., Vignati, E., Wilson, J., Ganzeveld, L., Tegen, I., Werner, M., Balkanski, Y., Schulz, M., Boucher, O., Minikin, A., and Petzold, A.: The aerosol-climate model ECHAM5-HAM, Atmos. Chem. Phys., 5, 1125-1156, doi:10.5194/acp-5-1125-2005, 2005.

Textor, C., Schulz, M., Guibert, S., Kinne, S., Balkanski, Y., Bauer, S., Berntsen, T., Berglen, T., Boucher, O., Chin, M., Dentener, F., Diehl, T., Easter, R., Feichter, H., Fillmore, D., Ghan, S., Ginoux, P., Gong, S., Grini, A., Hendricks, J., Horowitz, L., Huang, P., Isaksen, I., Iversen, I., Kloster, S., Koch, D., Kirkevag, A., Kristjansson,J. E., Krol, M., Lauer, A., Lamarque, J. F., Liu, X., Montanaro, V., Myhre, G., Penner, J., Pitari, G., Reddy, S., Seland, Ø., Stier, P., Takemura, T., and Tie, X.: Analysis and quantification of the diversities of aerosol life cycles within AeroCom, Atmos. Chem. Phys., 6, 1777–1813, doi:10.5194/acp-6-1777-2006, 2006.

Tsigaridis. K., Krol, M., Dentener, F. J., Balkanski, Y., Lathiere, J., Metzger, S., Hauglustaine, D. A., and Kanakidou, M.: Change in global aerosol composition since preindustrial times, Atmos. Chem. Phys., 6, 5143-5162, 2006.

Usoskin, I. G. and Kovaltsov, G. A.: Cosmic ray induced ionization in the atmosphere: full modeling and practical applications, J. Geophys. Res., 111, D21206, doi:10.1029/2006JD007150, 2006.

van Dingenen, R. and Raes, F.: Ternary nucleation of methane sulphonic acid, sulphuric acid and water vapour, J. Aerosol Sci., 24, 1-17, doi:10.1016/0021-8502(93)90081-J, 1993.

Van Pelt, R. S. and Zobeck, T. M.: Chemical constituents of fugitive dust, Environ. Monit. Assess., 130, 3-16, doi:10.1007/s10661-006-9446-8, 2007.

Vehkamaki, H., Kulmala, M., Napari, I., Lehtinen, K. E. J., Timmreck., C., Noppel, M., and Laaksonen, A.: an improved parameterization for sulfuric acid-water nucleation rates for tropospheric and stratospheric conditions, Journal of Geophysical Research-Atmospheres, 107(D22), 4622, doi:10.1029/2002JD002184, 2002.

Wang, M. and Penner, J. E.: Aerosol indirect forcing in a global model with particle nucleation, Atmos. Chem. Phys., 9, 239-260, 2009.

Wang, K., Zhang, Y., Nenes, A., and Fountoukis, C.: Implementation of dust emission and chemistry into the Community Multiscale Air Quality modeling system and initial application to an Asian dust storm episode, Atmos. Chem. Phys., 12, 10209-10237, doi:10.5194/acp-12-10209-2012, 2012.

1203 Williams, J. E., Scheele, M. P., van Velthoven, P. F. J., Cammas, J.-P., Thouret, V. Galy-Lacaux,
1204 C., and Volz-Thomas, A.: The influence of biogenic emissions from Africa on tropical
1205 tropospheric ozone during 2006: a global modeling study, Atmos. Chem. Phys., 9, 5729-5749,
1206 2009.

1207 Yu, F.: From molecular clusters to nanoparticles: Second generation ion-mediated nucleation
1208 model, Atmos. Chem. Phys., 6, 5193-5211, 2006.

1209 Yu, F.: Ion-mediated nucleation in the atmosphere: Key controlling parameters, implications, and
1210 look-up table, J. Geophys. Res., 115, D03206, doi: 10.1029/2009JD012630, 2010.

1211 Yu, F., Luo, G., Liu, X., Easter, R. C., Ma, X., and Ghan, S. J.: Indirect radiative forcing by ion-
1212 mediated nucleation of aerosol, Atmos. Chem. Phys., 12, 11451-11463, 2012.

1213 Yu, F., Wang, Z., Luo, G., and Turco, R. P.: Ion-mediated nucleation as an important global
1214 source of tropospheric aerosols, Atmos. Chem. Phys., 8, 2537-2554, 2008.

1215 Zaveri, R. A., Easter, R. C., and Peters, L. K.: A computationally efficient multicomponent
1216 equilibrium solver for aerosols (MESA), J. Geophys. Res., 110, D24203, doi:
1217 10.1029/2004JD005618, 2005.

1218 Zender, C. S., Bian, H., and Newman, D.: The mineral Dust Entrainment And Deposition
1219 (DEAD) model: Description and 1990s dust climatology, J. Geophys. Res., 108(D14), 4416,
1220 doi: 10.1029/2002JD002775, 2003.

1221 Zhang, G. J., and McFarlane, N. A.: Sensitivity of climate simulations to the parameterization of
1222 cumulus convection in the Canadian Climate Centre general circulation model, Atmosphere-
1223 Ocean, 33, 407-446, 1995.

1224 Zhang, K. M., and A. S. Wexler: An Asynchronous Time-Stepping (ATS) integrator for atmospheric
1225 applications: Aerosol dynamics, Atmos. Environ., 40, 4574–4588, 2006.

1226 Zaveri, R. A., R. C. Easter, J. D. Fast, and L. K. Peters: Model for Simulating Aerosol Interactions and
1227 Chemistry (MOSAIC), J. Geophys. Res., 113, D13204, doi:10.1029/2007JD008782, 2008.

1228 Zhang, Y., Bischof, C. H., Easter, R. C., and Wu, P.-T.: Sensitivity analysis of a mixed-phase
1229 chemical mechanism using automatic differentiation, J. Geophys. Res., 103 (D15), 18,953-
1230 18,979, 1998.

1231 Zhang, Y., Seigneur, C., Seinfeld, J. H., Jacobson, M., Clegg, S. L., Binkowski, F. S.: A
1232 comparative review of inorganic aerosol thermodynamic equilibrium modules: similarities,
1233 differences, and their likely causes, Atmos. Environ., 34, 117-137, 2000.

1234 Zhang, Y., Pun, B., Vijayaraghavan, K., Wu, S.-Y., Seigneur, C., Pandis, S. N., Jacobson, M. Z.,
1235 Nenes, A., and Seinfeld, J. H.: Development and application of the Model of Aerosol Dynamics,
1236 Reaction, Ionization, and Dissolution (MADRID), J. Geophys. Res., 109, D01202,
1237 doi:10.1029/2003JD003501, 2004.

1238 Zhang, Y., McMurry, P. H., Yu, F., and Jacobson, M. Z.: A comparative study of nucleation
1239 parameterizations: 1. Examination and evaluation of the formulations, J. Geophys. Res., 115,
1240 D20212, doi: 10.1029/2010JD014150, 2010.

1241 Zhang, Y., Chen, Y., Sarwar, G., and Schere, K.: Impacts of gas-phase mechanisms on weather
1242 research forecasting model with chemistry (WRF/Chem) predictions: Mechanism
1243 implementation and comparative evaluation, J. Geophys. Res., 117, D01301, doi:
1244 10.1029/2011JD015775, 2012a.

1245 Zhang, Y., Karamchandani, P., Glotfelty, T., Street, D. G., Grell, G., Nenes, A., Yu, F., and
1246 Bennartz, R.: Development and initial application of the global-through-urban weather
1247 research and forecasting model with chemistry (GU-WRF/Chem), J. Geophys. Res., 117,
1248 D20206, doi:10.1029/2012JD017966, 2012b.

1249 Zuend, A., Marcolli, C., Peter, T., and Seinfeld, J. H.: Computation of liquid-liquid equilibria and
1250 phase stabilities: implications for RH-dependent gas/particle partitioning of organic-inorganic
1251 aerosols, Atmos. Chem. Phys., 10, 7795-7820, doi:10.5194/acp-10-7795-2010, 2010.

Table 1. Simulation design and purposes

Run Index	Model Configuration	Purpose
MAM_SIM	Simple gas-phase chemistry coupled with default MAM7	A baseline run for the 1st set of simulations (see text)
MAM_CB05_GE	CB05_GE coupled with default MAM7	Differences of MAM_SIM and MAM_CB05_GE indicate the impacts of gas-phase chemical mechanisms
MAM_CON	Same as MAM_CB05_GE, but with explicit treatments for NO_3^-, Cl^-, and Na^+; HNO_3 and HCl condensation and aqueous-phase chemistry; species-dependent accommodation coefficients	A baseline run for the 2nd set of simulations; differences of MAM_SIM and MAM_CB05_GE indicate the impact of modified condensation and aqueous-phase chemistry treatments
MAM_CON/IMN	Same as MAM7_CON, but combine IMN with modified default nucleation parameterizations with a prefactor of 1.0×10^{-8}	Differences of MAM_CON and MAM_CON/IMN indicate the impacts of IMN and the lower prefactor for WP09
MAM_CON/ISO	Same as MAM7_CON, but with ISORROPIA II for aerosol thermodynamics under metastable conditions	Differences between MAM_CON and MAM_IMN/ISO indicate the impacts of explicit aerosol thermodynamics
MAM_NEWA	Same as MAM7_CON, but with all modified and new treatments and using a prefactor of 1.0×10^{-9} for default nucleation parameterization	Differences between MAM_CB05_GE and MAM_NEWA indicate the impacts of all new and modified treatments for inorganic aerosols
MAM_NEWB	Same as MAM_NEWA, but with ISORROPIA II under stable condition	Differences between MAM_NEWA and MAM_NEWB indicate the impacts of thermodynamic conditions on gas-aerosol partitioning
MAM_NEW/EMIS	Same as MAM7_NEW, but with adjusted emissions of SO_2, NH_3, BC, POM, and CO over CONUS, Europe, and East Asia	Differences between MAM_NEWA and MAM_NEW/EMIS indicate the impact of emissions
MAM_SIM_5Y	Same as MAM_SIM, but with prescribed SST for 2001-2005	A baseline run for 4th set of simulations
MAM_NEW_5YA	Same as MAM_NEW/EMIS, but with prescribed SST for 2001-2005	Differences between MAM_SIM_5Y and MAM_NEW_5YA indicate the indicate the impacts of all new and modified treatments for inorganic aerosols
MAM_NEW_5YB	Same as MAM_NEW/EMIS, but with fully-coupled model for 2001-2005	Difference between MAM_NEW_5YB and MAM_NEW_5YA indicate the impacts of processes from component models in the fully-coupled Earth system

Table 2. Mean Bias (MB) and Normalized Mean Bias (NMB, in %) of Radiative/Cloud Predictions for the 2001 Simulations

Species/Variables	Dataset	Obs.	Simulations						
			MAM_ SIM	MAM_ CB05_GE	MAM_ CON	MAM_ CON/IMN	MAM_ CON/ISO	MAM_ NEWA	MAM_ NEW/EMIS
LWD (W m^{-2})[a]	BSRN	312.5	309.2/ -3.4/-1.1[c]	309.6/ -2.9/-0.9	308.4/ -4.2/-1.3	308.0/ -4.5/-1.4	308.3/ -4.2/-1.3	308.7/ -3.8/-1.2	309.1/ -3.5/-1.1
SWD (W m^{-2})[b]	BSRN	181.2	179.2/ -2.0/-1.1	177.0/ -4.2/-2.3	169.4/ -11.8/-6.5	170.2/ -11.0/-6.1	177.3/ -3.9/-2.2	174.5/ -6.8/-3.7	177.0/ -4.2/-2.3
OLR (W m^{-2})	NOAA-CDC	214.4	223.2/ 8.8/4.1	222.4/ 8.1/3.8	219.3/ 4.9/2.3	219.3/ 4.9/2.3	220.7/ 6.2/2.9	221.2/ 6.9/3.2	221.2/ 6.9/3.2
SWCF (W m^{-2})	CERES	-41.0	-37.8/ -3.2/-7.9	-38.4/ -2.7/-6.5	-43.2/ 2.2/5.3	-43.3/ 2.3/5.6	-40.4/ -0.7/-1.6	-40.7/ -0.4/-0.9	-40.5/ -0.6/-1.4
CF (%)	MODIS	66.9	65.6/ -1.4/-2.0	65.9/ -1.0/-1.5	67.5/ 0.5/0.8	67.6/ 0.7/1.0	66.4/ -0.5/-0.8	66.5/ -0.4/-0.6	66.6/ -0.3/-0.5
COT	MODIS	17.1	6.9/ -10.2/-59.5	7.1/ -10.1/-58.8	8.7/ -8.4/-49.2	8.8/ -8.3/-48.4	7.7/ -9.4/-55.1	7.7/ -9.4/-54.9	7.7/ -9.4/-55.2
CWP (g m^{-2})	MODIS	148.1	33.0/ -115.1/ -77.7	33.5/ -114.7/ -77.4	42.3/ -105.8/ -71.4	42.7/ -105.4/ -71.2	36.4/ -111.7/ -75.4	36.5/ -111.7/ -75.4	36.2/ -111.9/ -75.5
PWV (cm)	MODIS	1.9	1.9/ -2.5×10^{-2}/ -1.3	1.9/ -1.8×10^{-2}/ -0.9	1.9/ -3.3×10^{-2}/ -1.7	1.9/ -3.9×10^{-2}/ -2.0	1.9/ -1.8×10^{-2}/ -0.9	1.9/ -1.4×10^{-2}/ -0.7	1.9/ -1.2×10^{-2}/ -0.6
AOD	MODIS	1.5×10^{-1}	9.8×10^{-2}/ -5.5×10^{-2}/ -36.1	1.0×10^{-1}/ -5.2×10^{-2}/ -33.9	1.2×10^{-1}/ -3.0×10^{-2}/ -19.8	1.3×10^{-1}/ -2.6×10^{-2}/ -17.1	1.0×10^{-1}/ -5.3×10^{-2}/ -34.4	1.0×10^{-1}/ -5.0×10^{-2}/ -32.9	1.0×10^{-1}/ -5.2×10^{-2}/ -34.0
Column CCN5 (ocean) (cm^{-2})	MODIS	2.4×10^{8}	5.8×10^{7}/ -1.9×10^{8}/ -76.4	5.2×10^{7}/ -1.9×10^{8}/ -78.6	1.8×10^{8}/ -6.7×10^{7}/ -27.5	2.0×10^{8}/ -4.6×10^{7}/ -18.8	9.1×10^{7}/ -1.5×10^{8}/ -62.7	8.5×10^{7}/ -1.6×10^{8}/ -65.3	8.2×10^{7}/ -1.6×10^{8}/ -66.6
CDNC (cm^{-3})	BE07	113.1	45.5/ -67.7/-59.9	46.7/ -66.5/-58.8	89.7/ -23.4/-20.7	93.1/ -20.0/-17.7	65.0/ -48.1/-42.5	66.7/ -46.4/-41.0	67.0/ -46.1/-40.8

[a]The pair of observation and simulation is removed in the statistical calculation if the observed LWD value is lower than 50 W m^{-2} or higher than 700 W m^{-2} (http://www.pangaea.de).

[b]The pair of observation and simulation is removed in the statistical calculation if the observed SWD value is lower than -10 or higher than 3000 W m^{-2} (http://www.pangaea.de).

[c]The values of modeled results (Sim), MBs, and NMBs are expressed as Sim/MB/NMB.

Table 3. Mean Bias (MB) and Normalized Mean Bias (NMB, in %) of Chemical Predictions for the 2001 Simulations

Species/ variables[a]	Domain	Obs.	Simulations							
			MAM_SIM	MAM_CB05_GE	MAM_CON	MAM_CON/IMN	MAM_CON/ISO	MAM_NEWA	MAM_NEWB	MAM_NEW/ EMIS
CO	Europe	123.0	-	112.4/-10.6/-8.6	115.0/-8.0/-6.5	107.9/-15.1/-12.3	114.0-9.0/-7.3	118.8/-4.2/-3.4	113.6/-9.4/-7.6	137.9/14.9/12.1
	East Asia	0.6	-	0.1/-0.5/-82.1	0.1/-0.5/-82.0	0.1/-0.5/-81.8	0.1/-0.5/-81.8	0.1/-0.5/-82.0	0.1/-0.5/-81.7	0.1/-0.5/-78.7
SO_2	CONUS	3.9	14.2/10.3/264.8[b]	14.4/10.5/270.1	15.6/11.7/301.2	15.1/11.2/286.1	15.4/11.5/295.8	15.3/11.4/291.8	15.3/11.4/293.0	9.8/5.9/152.2
	Europe	6.8	13.4/6.6/97.5	13.8/7.0/103.2	15.2/8.4/123.0	13.6/6.8/100.3	14.6/7.8/114.7	15.7/8.9/130.7	14.5/7.7/114.0	6.8/0.0/0.3
	East Asia	12.5	4.6/-7.9/-63.0	4.8/-7.7/-61.3	4.8/-7.7/-61.4	4.8/-7.7/-61.8	4.9-7.6/-61.0	4.8/-7.7/-61.2	4.8/-7.7/-61.2	5.8/-6.7/-53.4
NH_3	Europe	9.4	1.7/-7.7/-82.0	1.8/-7.6/-80.8	1.2/-8.2/-86.8	1.1/-8.3/-87.8	1.4/-8.0/-84.7	1.5/-7.9/-84.3	1.1/-8.3/-84.0	2.1/-7.3/-77.5
NO_2	Europe	20.2	-	4.6/-15.6/-77.0	5.2/-15.0/-74.1	4.7/-15.5/-76.5	5.0/-15.2/-75.2	5.2/-15.0/-74.1	4.9/-15.3/-75.7	4.9/-15.3/-75.9
	East Asia	14.0		1.6/-12.4/-88.4/	1.7/-12.3/-88.0	1.7/-12.3/-88.2	1.6/-12.4/-88.4	1.7/-12.3/-88.3	1.6/-12.4/-88.5	1.7/-12.3/-88.2
O_3	CONUS	34.6	-	44.6/10.0/28.9	42.6/8.0/23.0	42.5/7.9/22.7	44.4/9.8/28.4	44.1/9.5/27.4	43.7/9.1/26.4	44.4/9.8/28.1
	Europe	53.5	-	90.2/36.7/68.6	84.4/30.9/57.7	84.5/31.0/58.0	87.6/34.1/63.7	87.0/33.5/62.7	87.7/34.2/63.9	88.4/34.9/65.2
	East Asia	26.4		42.8/16.4/62.2	42.7/16.3/61.7	40.7/14.3/54.3	42.6/16.2/65.9	42.1/15.7/59.6	43.0/16.6/63.0	42.5/16.1/61.2
HNO_3	CONUS	1.5	-	2.5/1.0/68.1	0.6/-0.9/-60.2	0.6/-0.9/-59.7	1.7/0.2/15.8	1.8/0.3/17.7	1.8/0.3/19.0	1.6/0.1/4.1
	Europe	0.5	-	1.8/1.3/268.5	0.3/-0.2/-34.1	0.3/-0.2/-35.8	0.9/0.4/86.1	0.9/0.4/83.6	1.0/0.5/103.8	0.9/0.4/73.8
SO_4^{2-}	CONUS	2.6	2.5/-0.1/-5.1	2.4/-0.2/-7.2	$2.6/4.4\times10^{-2}$/1.7	$2.6/4.2\times10^{-2}$/1.6	2.4/-0.2/-7.9	2.4/-0.2/-6.3	2.5/-0.1/-5.5	1.9/-0.7/-28.4
	Europe	2.2	3.0/0.8/36.5	2.9/0.7/33.1	3.1/0.9/40.3	3.0/0.8/35.8	2.9/0.7/32.6	3.1/0.9/39.4	3.0/0.8/36.8	2.0/-0.2/-7.2
NH_4^+	CONUS	1.4	1.0/-0.4/-32.1	0.8/-0.6/-39.6	1.7/0.3/20.0	1.7/0.3/19.7	1.3/-0.1/-6.4	1.3/-0.1/-6.5	1.3/-0.1/-4.3	1.2/-0.2/-13.1
	Europe	1.2	1.1/-0.1/-9.1	1.0/-0.2/18.3	2.2/1.0/85.0	2.0/0.8/65.7	1.8/0.6/49.4	1.9/0.7/54.8	1.7/0.5/37.7	1.6/0.4/32.5
NO_3^-	CONUS	1.0	-	-	3.0/2.0/198.2	2.9/1.9/192.7	$1.0/-4.8\times10^{-2}$/-4.8	0.9/-0.1/-9.6	$1.0/-2.2\times10^{-2}$/-2.1	$1.0/4.0\times10^{-3}$/0.4
	Europe	2.0	-	-	3.4/1.4/67.8	3.0/1.0/49.4	1.9/-0.1/-4.3	$2.0/-4.0\times10^{-2}$/-2.0	1.8/-0.2/-12.5	2.1/0.1/5.2
Cl^-	CONUS	0.1	-	-	0.5/0.4/359.9	0.5/0.4/373.1	$0.1/-1.5\times10^{-2}$/-14.5	$0.1/-1.8\times10^{-2}$/-17.5	$0.1/-1.5\times10^{-2}$/-12.1	$0.1/-2.8\times10^{-3}$/-2.8
	Europe	0.7	-	-	1.4/0.7/102.8	1.3/0.6/89.9	$0.7/2.1\times10^{-3}$/0.3	$0.7/1.4\times10^{-2}$/2.0	0.6/-0.1/-14.5	-4.7×10^{-2}/-6.7
BC	CONUS	0.6	0.3/-0.3/-54.6	0.3/-0.3/-55.8	0.3/-0.3/-54.7	0.3/-0.3/-54.6	0.3/-0.3/-53.8	0.3/-0.3/-54.3	0.3/-0.3/-54.9	0.4/-0.2/-29.4
OC	CONUS	1.1	0.8/-0.3/-22.7	1.0/-0.1/-12.1	1.0/-0.1/-11.4	1.0/-0.1/-11.9	1.0/-0.1/-8.6	1.0/-0.1/-9.1	1.0/-0.1/-11.3	$1.0/5.6\times10^{-3}$/0.5
TC	CONUS	2.5	1.3/-1.2/-47.9	1.4/-1.1/-43.1	1.4/-1.1/-42.2	1.4/-1.1/-42.5	1.4/-1.0/-40.9	1.5/-1.0/-41.1	1.4/-1.1/-42.5	1.6/-0.9/-35.0
$PM_{2.5}$	CONUS	7.9	4.9/-3.0/-37.6	5.0/-2.9/-36.8	9.5/1.6/20.1	6.6/1.3/16.7	7.8/-0.1/-1.7	6.9/-1.0/-13.2	7.2/-0.7/-8.8	6.8/-1.1/-13.5
	Europe	14.5	8.4/-6.1/-41.8	7.9/-6.6/-45.3	13.7/-0.8/-5.5	14.4/-0.1/-0.9	11.0/-3.5/-24.4	11.9/-2.6/-17.7	10.9/-3.6/-24.9	10.6/-3.9/-27.2
PM_{10}	Europe	25.7	17.5/-8.2/-31.8	16.5/-9.2/-35.8	22.5/-3.2/-12.3	23.0/-2.7/-10.5	20.1/-4.8/-18.5	21.4/-4.3/-16.6	20.7/-5.0/-19.4	20.9/-4.8/-18.8
	East Asia	118.5	38.5/-80.0/-67.5	44.9/-73.6/-62.1	55.9/-62.6/-52.8	58.8/-57.7/-48.7	48.5/-70.0/-59.1	65.5/-53.0/-44.7	55.6/-62.9/-53.1	48.2/-70.3/-59.3
Col.CO	Globe	1.3×10^{18}	- --	1.2×10^{18}/ -7.4×10^{16}/-5.7	1.2×10^{18}/ -5.7×10^{16}/-4.4	1.2×10^{18}/ -6.3×10^{16}/-4.8	1.2×10^{18}/ -6.4×10^{16}/-4.9	1.2×10^{18}/ -6.3×10^{16}/-4.8	1.2×10^{18}/ -5.6×10^{16}/-4.3	1.3×10^{18}/ 2.3×10^{16}/1.8
Col.NO_2	Globe	4.7×10^{14}	-	6.7×10^{14}/ 1.9×10^{14}/40.5	6.2×10^{14}/ 1.4×10^{14}/30.4	6.2×10^{14}/ 1.4×10^{14}/30.0	6.5×10^{14}/ 1.8×10^{14}/37.5	6.5×10^{14}/ 1.8×10^{14}/37.2	6.5×10^{14}/ 1.8×10^{14}/37.9	6.5×10^{14}/ 1.8×10^{14}/37.3
TOR	Globe	30.3	29.8/-0.5/1.6	29.2/-1.1/-3.7	27.6/-2.7/-9.0	27.4/-2.9/-9.6	28.8/-1.5/-4.9	28.7/-1.6/-5.2	28.6/-1.5/-5.0	28.6-1.5/-4.9
J	Globe	0.6	0.003/-0.6/-99.6	0.1/-0.5/-99.5	0.5/-0.1/-12.8	0.3/-0.3/-49.6	0.8/0.2/36.1	0.3/-0.3/-53.1	0.3/-0.3/-51.7	0.3/-0.3/-62.0

[a]The units are CO, ppb (over Europe) and ppm (over East Asia); SO_2, ppb (over East Asia) and μg m^{-3} (over CONUS and Europe); O_3, ppb (over CONUS) and μg m^{-3} (over Europe); column CO and NO_2, molecules cm^{-2}; TOR, DU; J, $cm^{-3}s^{-1}$. All other concentrations are in μg m^{-3}. [b]The values of modeled results (Sim), MBs, and NMBs are expressed as Sim/MB/NMB.

Table 4. The observed values and the mean bias (MB) and normalized mean bias (NMB, in %) of predictions of O_3 NO_2, and HNO_3 mixing ratios over Europe in MAM_NEWA

	Network		Obs ($\mu g\ m^{-3}$)	Sim ($\mu g\ m^{-3}$)	MB/NMB
Winter	Airbase			75.2	37.5/99.6[a]
		NO_2	26.0	7.6	-18.4/-70.9
	BDQA	O_3	31.0	74.2	43.2/139.2
		NO_2	30.6	5.6	-25.0/-81.9
	EMEP	O_3	50.7	75.7	25.0/49.3
		NO_2	9.0	8.3	-0.7/-7.8
		HNO_3	0.5	0.5	-4.9×10^{-3}/1.0
Spring	Airbase	O_3	63.1	100.8	37.7/59.7
		NO_2	20.0	4.6	-15.4/-77.1
	BDQA	O_3	59.6	98.9	39.3/65.9
		NO_2	23.6	3.1	-20.5/-87.0
	EMEP	O_3	75.0	101.9	26.9/35.9
		NO_2	5.9	4.9	-1.0/-17.2
		HNO_3	0.4	0.9	0.5/144.5
Summer	Airbase	O_3	64.9	93.5	28.6/44.0
		NO_2	16.2	4.4	-11.8/-72.8
	BDQA	O_3	64.5	94.5	30.0/46.5
		NO_2	18.7	3.6	-15.1/-80.9
	EMEP	O_3	72.2	91.2	19.0/26.3
		NO_2	4.7	4.4	-0.3/-6.2
		HNO_3	0.5	1.3	0.8/169.6
Autumn	Airbase	O_3	40.5	79.5	39.0/96.4
		NO_2	21.7	5.3	-16.4/-75.6
	BDQA	O_3	35.7	80.9	45.2/126.5
		NO_2	24.8	3.7	-21.1/-85.2
	EMEP	O_3	51.7	78.2	26.5/51.2
		NO_2	6.6	5.2	-1.4/-21.1
		HNO_3	0.6	0.9	0.3/45.0

[a]The values of MBs and NMBs are expressed as MB/NMB.

Table 5. Statistical Performance of Radiative/Cloud Predictions (Average of the 5-yr (2001-2005) Simulations)

Species/Variables	Dataset	Obs.	Simulations		
			MAM_SIM_5Y	MAM_NEW_5YA	MAM_NEW_5YB
LWD (W m^{-2})[a]	CERES	307.6	302.9/-4.7/-1.5/2.9/11.6[c]	303.9/-3.6/-1.1/2.8/11.3	304.4/-3.1/-1.0/2.9/11.3
SWD (W m^{-2})[b]	CERES	163.9	169.9/5.9/3.6/7.0/14.1	166.5/2.5/1.5/6.5/13.8	167.0/3.1/1.9/6.7/13.7
OLR (W m^{-2})	NOAA-CDC	215.9	222.5/6.6/3.1/3.5/8.9	220.7/4.8/2.2/3.4/9.1	221.4/5.5/2.6/3.5/9.0
SWCF (W m^{-2})	CERES	-41.0	-38.8/2.2/-5.4/-21.5/12.0	-41.5/-0.5/1.2/-21.4/12.5	-40.8/0.2/-0.5/-22.2/12.4
CF (%)	MODIS	67.1	66.6/-0.6/-0.8/15.2/13.3	67.3/0.2/0.3/14.7/13.0	66.6/-0.6/-0.9/15.5/13.7
COT	MODIS	17.3	7.1/-10.3/-59.3/70.2/15.1	7.9/-9.4/-54.5/65.7/14.6	7.8/-9.6/-55.2/65.6/14.5
CWP (g m^{-2})	MODIS	86.0	38.2/-47.8/-55.5/55.7/52.9	43.2/-42.8/-49.8/50.0/49.2	43.4/-42.6/-49.5/49.7/49.2
PWV (cm)	MODIS	1.93	1.96/0.03/1.5/11.6/0.3	1.99/0.06/2.9/10.9/0.3	1.97/0.04/1.8/13.8/0.3
AOD	MODIS	0.2	0.1/-0.07/-44.1/54.5/0.1	0.1/-0.06/-39.2/51.3/0.1	0.1/-0.06/-36.3/49.5/0.1
Column CCN5 (ocean) (cm^{-2})	MODIS	2.5×10^8	5.3×10^7/-1.9×10^8/ -78.6/78.6/5.7×10^8	8.6×10^7/1.6×10^8/ -65.2/65.2/5.5×10^8	8.6×10^7/1.6×10^8/ -65.3/65.3/5.5×10^8
CDNC (cm^{-3})	BE07	112.6	44.2/-68.3/-60.7/61.6/84.3	69.2/-43.4/-38.6/44.2/66.8	68.8/-43.8/-38.9/45.5/67.9

[a] The pair of observation and simulation is removed in the statistical calculation if the observed LWD value is lower than 50 W m^{-2} or higher than 700 W m^{-2} (http://www.pangaea.de).

[b]The pair of observation and simulation is removed in the statistical calculation if the observed SWD value is lower than -10 or higher than 3000 W m^{-2} (http://www.pangaea.de).

[c]The values are expressed as Sim/MB/NMB/NME/RMSE. Sim: simulated values; MB: mean bias; NMB: normalized mean bias (%); NME: normalized mean error (%); RMSE: root mean squared error.

Table 6. Statistical Performance of Chemical Predictions (Average of from the 5-yr (2001-2005) Simulations)

Species/ variables[a]	Domain	Obs.	Simulations		
			MAM_SIM_5Y	MAM_NEW_5YA	MAM_NEW_5YB
CO	East Asia	562.0	-	139.7/-422.3/-75.1/75.1/451.8[b]	137.0/-425.0/-75.6/75.6/454.0
SO_2	CONUS	3.4	9.6/6.2/183.9/184.6/9.9	10.1/6.7/198.8/199.1/10.6	10.3/6.9/203.1/203.5/10.9
	Europe	6.6	6.0/-0.6/-9.3/73.3/7.9	6.6/-0.06/-0.9/77.2/8.3	6.2/-0.4/-5.5/74.6/8.0
	East Asia	3.4	3.4/0.04/1.1/76.0/5.0	3.4/0.01/0.4/76.2/5.0	3.4/-0.05/-1.6/73.1/4.8
NH_3	Europe	6.3	3.0/-3.3/-52.0/81.0/25.3	2.4/-3.9/-61.3/79.7/25.3	2.4/-3.9/-62.0/79.3/25.3
NO_2	Europe	23.5	-	5.8/-17.7/-75.4/76.5/21.5	5.5/-18.0/-76.7/77.7/21.7
	East Asia	13.5	-	2.3/-11.2/-83.3/83.3/12.2	2.3/-11.2/-83.6/83.6/12.2
O_3	CONUS	35.1	-	43.9/8.8/25.1/27.3/11.3	44.1/9.0/25.7/27.7/11.6
	Europe	52.7	-	86.6/33.9/64.5/64.6/36.4	89.2/36.5/69.3/69.4/38.8
	East Asia	27.4	-	45.6/18.2/66.4/66.4/19.2	45.5/18.1/66.0/66.0/19.1
HNO_3	CONUS	1.4	-	1.6/0.2/16.3/39.5/0.7	1.6/0.2/12.1/38.2/0.7
	Europe	0.7	-	1.0/0.3/45.8/83.5/0.8	1.0/0.3/37.9/79.8/0.8
SO_4^{2-}	CONUS	2.6	2.3/-0.3/-13.4/26.9/1.0	2.3/-0.3/-13.1/23.0/0.8	2.3/-0.3/-12.8/24.2/0.9
	Europe	2.3	2.3/-0.04/-1.9/37.3/1.4	2.0/-0.3/-11.1/34.1/1.3	2.0/-0.3/-13.0/35.5/1.4
NH_4^+	CONUS	1.2	0.9/-0.3/-20.8/33.4/55.0	1.5/0.3/22.2/43.2/0.8	1.5/0.3/26.4/44.3/0.8
	Europe	1.0	0.8/-0.2/-16.8/36.9/0.5	1.6/0.6/62.8/68.7/0.9	1.5/0.5/53.8/60.3/0.8
NO_3^-	CONUS	1.1	-	1.6/0.5/41.3/85.4/1.4	1.6/0.5/49.8/90.2/1.5
	Europe	1.8	-	2.3/0.5/30.3/51.1/1.2	2.2/0.4/24.7/47.0/1.1
Cl^-	CONUS	0.1	-	$0.1/3.1\times10^{-3}$/2.7/105.8/0.4	$0.1/8.7\times10^{-3}$/7.8/110.1/0.4
	Europe	0.3	-	2.4/2.1/681.2/681.2/2.9	2.3/2.0/663.3/663.6/2.8
BC	CONUS	0.4	0.3/-0.1/-17.9/44.4/0.3	0.3/-0.1/-15.6/44.0/28.2	0.3/-0.1/-17.7/44.3/0.2
OC	CONUS	1.2	0.9/-0.3/-23.2/59.3/1.0	1.1/-0.1/-7.7/56.7/1.0	1.1/-0.1/-11.0/54.3/0.9
TC	CONUS	3.1	1.4/-1.7/-54.4/62.8/2.8	1.7/-1.4/-45.7/57.1/2.6	1.6/-1.5/-47.1/57.1/2.7
$PM_{2.5}$	CONUS	8.8	7.2/-1.6/-17.9/37.0/4.3	9.2/0.4/4.1/33.5/3.9	8.7/-0.1/-1.1/29.4/3.6
	Europe	14.6	6.7/-7.9/-53.9/54.6/10.6	9.7/-4.9/-33.8/37.6/8.6	10.0/-4.6/-31.7/36.1/8.4
PM_{10}	Europe	26.3	15.1/-11.2/-42.6/46.8/15.9	18.7/-7.6/-28.8/36.1/13.9	19.9/-6.4/-24.4/33.5/13.1
	East Asia	107.9	45.4/-62.5/-58.0/59.3/70.7	52.5/-57.4/-53.2/54.2/66.0	57.8/-50.1/-46.5/50.0/61.6
Col.CO	Globe	1.4×10^{18}	-	1.3×10^{18}/-1.4×10^{17}/ -10.2/16.5/3.1×10^{17}	1.2×10^{18}/-1.5×10^{17}/ -11.0/17.2/3.2×10^{17}
Col.NO_2	Globe	5.3×10^{14}	-	8.4×10^{14}/3.1×10^{14}/ 59.2/70.0/5.4×10^{14}	8.3×10^{14}/3.0×10^{14}/ 57.6/69.2/5.4×10^{14}
TOR	Globe	30.4	29.9/-0.5/1.6/16.3/6.1	30.5/0.1/0.4/15.0/5.8	29.9/-0.5/-1.7/16.4/6.1

[a]The units are CO, ppm (over East Asia); SO_2, ppb (over East Asia) and μg m^{-3} (over CONUS); O_3, ppb (over CONUS) and μg m^{-3} (over Europe); column CO and NO_2, molecules cm^{-2}; TOR, DU. All other concentrations are in μg m^{-3}.

[b]The values are expressed as Sim/MB/NMB/NME/RMSE. MB: mean bias; NMB: normalized mean bias (%); NME: normalized mean error (%); RMSE: root mean square error.

Table 7. Global Burdens of Major Gaseous and Aerosol Species from the 5-yr (2001-2005) Simulations

	MAM_SIM_5Y	MAM_NEW_5YA	Previous studies
Tropospheric CO (Tg) [a]	N.A.[c]	322.06	337-354 [d]
Tropospheric O_3 (DU) [a]	29.7 [c]	30.5	34.04 [e]
Tropospheric O_3 (Tg) [a]	324.14 [c]	332.87	372 [e]
DMS (Tg S)	0.051	0.058	0.067 [f]
SO_2 (Tg S)	0.276	0.281	0.34 [f]
H_2SO_4 (Tg S)	3.8×10^{-4}	1.9×10^{-3}	4.2×10^{-4} [f]
Tropospheric NO_x [a, b]	N.A. [c]	0.116 Tg N (8.24×10^{14} molecules cm^{-2})	7.6×10^{14} molecules cm^{-2} [g]
NOy (Tg N) [b]	N.A. [c]	3.26	N.A. [c]
NH3 (Tg N)	0.074	0.059	0.064 [f]
VOCs (Tg C) [b]	N.A. [c]	7.63	N.A. [c]
Tropospheric HCHO (Tg C) [a]	N.A. [c]	0.391	0.335-0.349 [d]
SO_4^{2-} (Tg S)	0.36	0.39	0.84 [e] ,0.47 [f], 0.66 [h]
NO_3^- (Tg N)	N.A. [c]	0.11	0.01-0.14 i
NH_4^+ (Tg N)	0.20	0.21	0.24 [f], (0.27-0.44) [i]
Na^+ (Tg)	2.93	3.04	2.98 [e], (0.38-5.19) [i]
Cl^- (Tg)	4.52	4.47	4.60 [e], (0.59-8.02) [i]
BC (Tg)	0.091	0.076	0.28 [e], 0.093 [f]
OC (Tg)	0.45	0.61	1.28 [e]
POM (Tg)	0.63	0.48	0.68 [f], 1.70 [h]
SOA (Tg)	N.A. [c]	0.38	1.15 [f], 0.59 [j]
Dust (Tg)	25.78	26.43	24.7 [f], (7.9-35.9) [i]

[a] CESM/CAM5 simulations use 30 model layers, with atmospheric pressures from ~1000 mb (layer 30) to ~3 mb (layer 1). Troposphere refers to model layers below tropopause height.

[b] $NO_x = NO + NO_2$; $NO_y = NO_x$ + nitrogen trioxide (NO_3) + dinitrogen pentoxide (N_2O_5) + nitrous acid (HONO) + nitric acid (HNO_3) + pernitric acid (HNO_4) + peroxyacyl nitrate (PAN) + $\geq C_3$ peroxyacyl nitrate (PANX) + other organic nitrate (NTR); VOCs-volatile organic compounds including acetaldehyde (ALD2), carboxylic acid(AACD), long-chain alkanes (ALKH), Cresol and higher phenols (CRES), ethene (ETH), ethane (ETHA), ethanol (ETOH), formaldehyde (FORM), internal olefinic carbon bond (IOLE), methanol (MEOH), olefinic carbon bond (OLE), paraffin carbon bond (PAR), polycyclic aromatic hydrocarbons (PAH), toluene (TOL), xylene (XYL), isoprene (ISOP), and terpene (TERP).

[c] N.A – not available, it refers to the species that are not treated in MAM_SIM_5Y or species having no burden data from previous studies. Tropospheric O_3 burden in MAM_SIM_5Y is from climatology. N.A. in SOA is due to no SOAG emission for MAM_SIM_5Y.

[d] Williams et al. (2009)

[e] Horowitz et al. (2006)

[f] Liu et al. (2012)

[g] Lamarque et al. (2006)

[h] Textor et al. (2006)

[i] Tsigaridis et al. (2006)

[j] Heald et al. (2008)

Figure captions

Figure 1a. Absolute differences of H_2O_2, SO_2, SO_4^{2-}, and SOA between MAM_CB05_GE and MAM_SIM for 2001.

Figure 1b. Absolute differences between the mixing ratios of surface OH, HO_2, NO_3, and O_3 predicted from MAM_CB05_GE and climatology values used in MAM_SIM for 2001.

Figure 2. Spatial distributions of CO, O_3, NO_2, HNO_3, HCl, and isoprene (ISOP) at surface simulated by MAM_CB05_GE for 2001.

Figure 3. Spatial distributions of total ammonium, total sulfate, total nitrate, total chloride, $PM_{2.5}$, NH_3, SO_2, H_2SO_4, HNO_3, and HCl at surface between MAM_CON and MAM_CB05_GE for summer (June, July, and August (JJA)), 2001.

Figure 4. Vertical distributions of new particle formation rate (J) (row 1) and aerosol number (PM_{num}) (row 3) simulated by MAM_CON/IMN for 2001. The overlay plots in row 2 show the distributions of simulated and observed J in bottom 1000-m in the atmosphere. Circles on overlay plots represent observations for J. Different colors of circles represent different values of J, using the same color scale as simulated J.

Figure 5. Absolute differences of $PM_{2.5}$, AOD, column CCN5, CF, COT, and SWCF between MAM_CON/IMN and MAM_CON for 2001.

Figure 6. Absolute differences of major PM species and their gas precursors between MAM_CON/ISO and MAM_CON for summer, 2001.

Figure 7. Absolute differences of major aerosol species and their gas precursors, new particle formation rate (J), and aerosol number between MAM_NEW_5YA and MAM_SIM_5Y for 2001-2005.

Figure 8. Absolute differences of major cloud and radiative variables between MAM_NEW_5YA and MAM_SIM_5Y for 2001-2005.

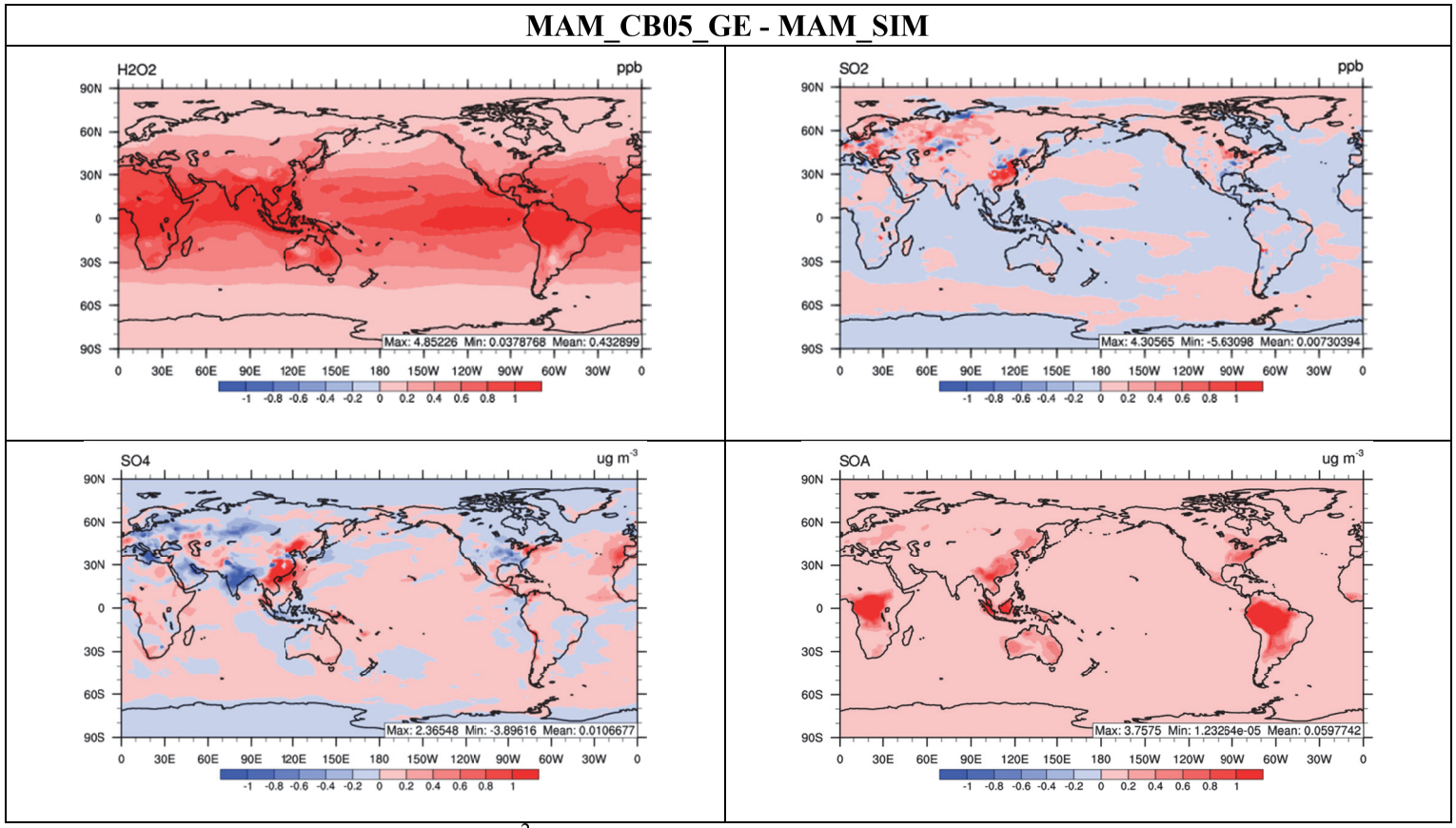

Figure 1a. Absolute differences of H_2O_2, SO_2, SO_4^{2-}, and SOA between MAM_CB05_GE and MAM_SIM for 2001.

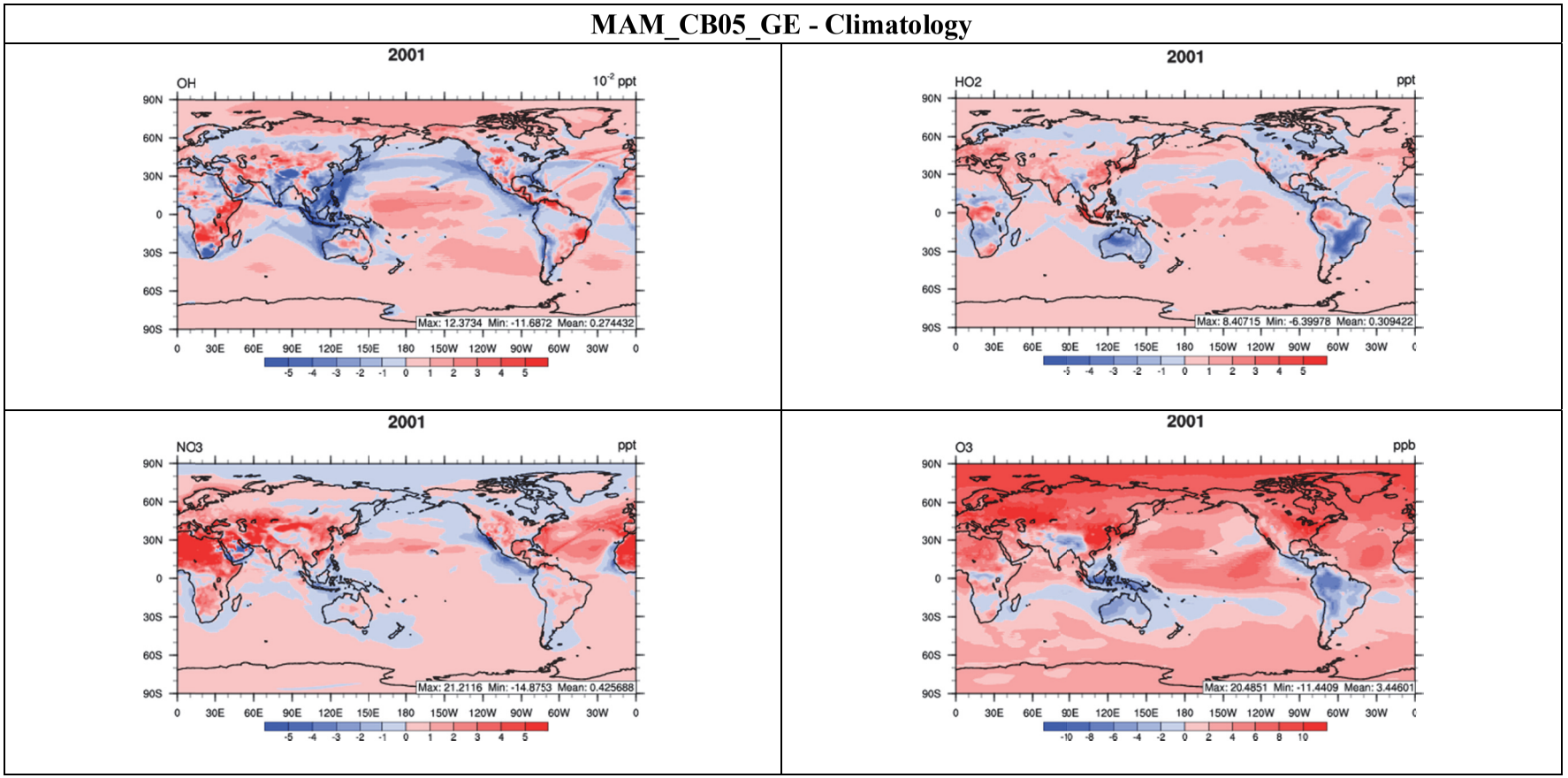

Figure 1b. Absolute differences between the mixing ratios of surface OH, HO_2, NO_3, and O_3 predicted from MAM_CB05_GE and climatology values used in MAM_SIM for 2001.

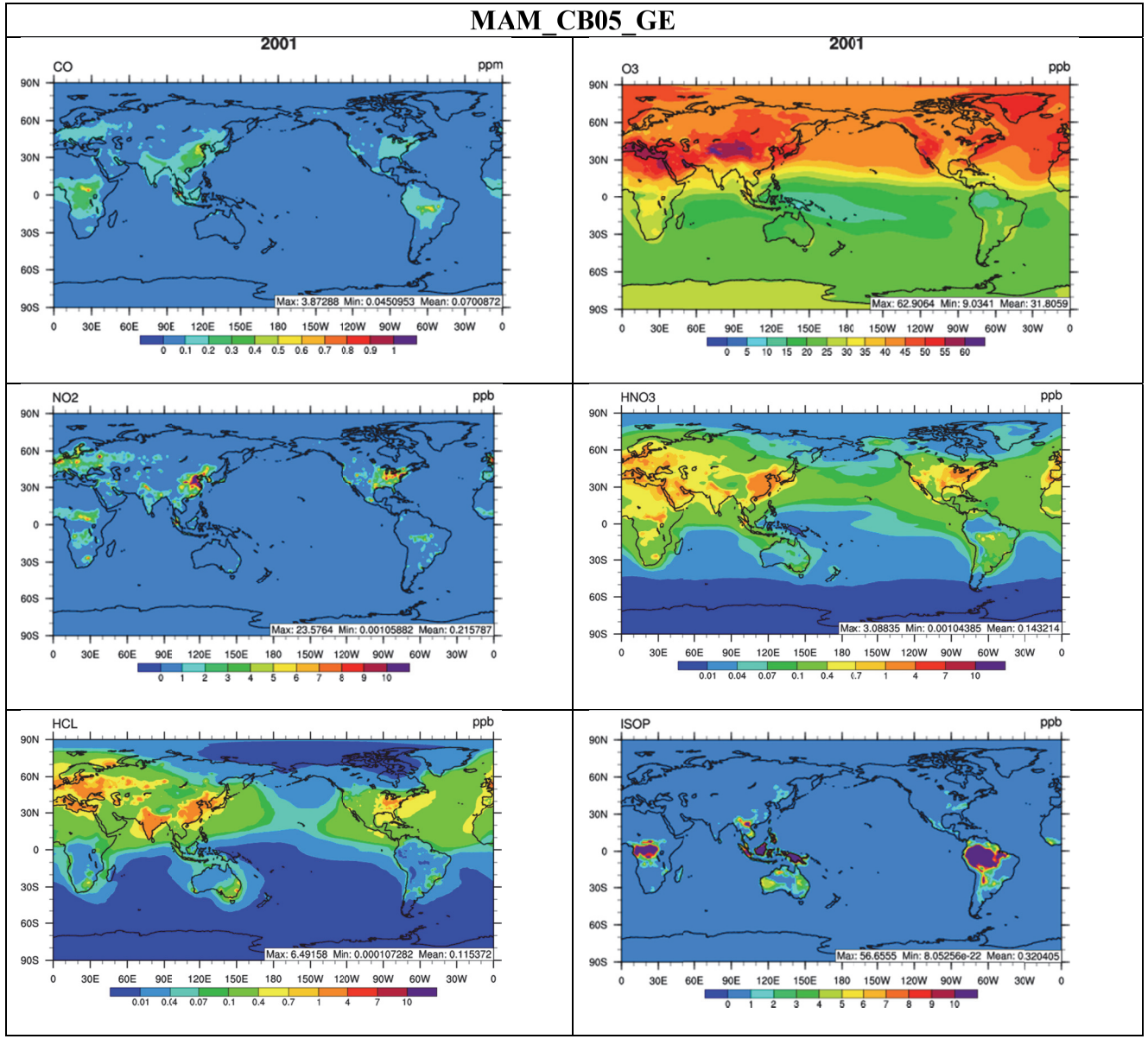

Figure 2. Surface distribution of CO, O_3, NO_2, HNO_3, HCl, and isoprene (ISOP) in MAM_CB05_GE for 2001.

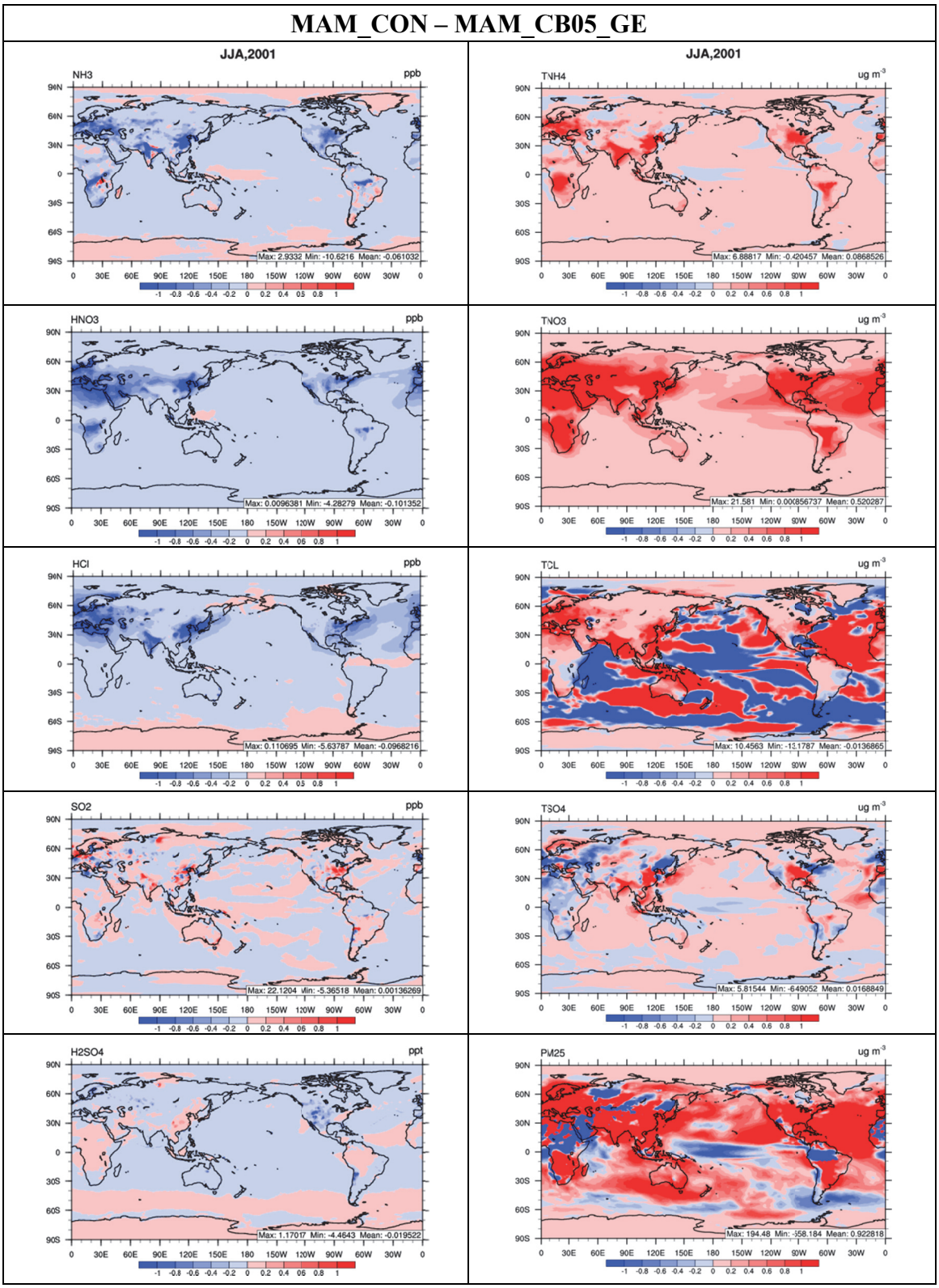

Figure 3. Surface distribution of total ammonium, total sulfate, total nitrate, total chloride, $PM_{2.5}$, NH_3, SO_2, H_2SO_4, HNO_3, and HCl between MAM_CON and MAM_CB05_GE for summer (June, July, and August (JJA)), 2001.

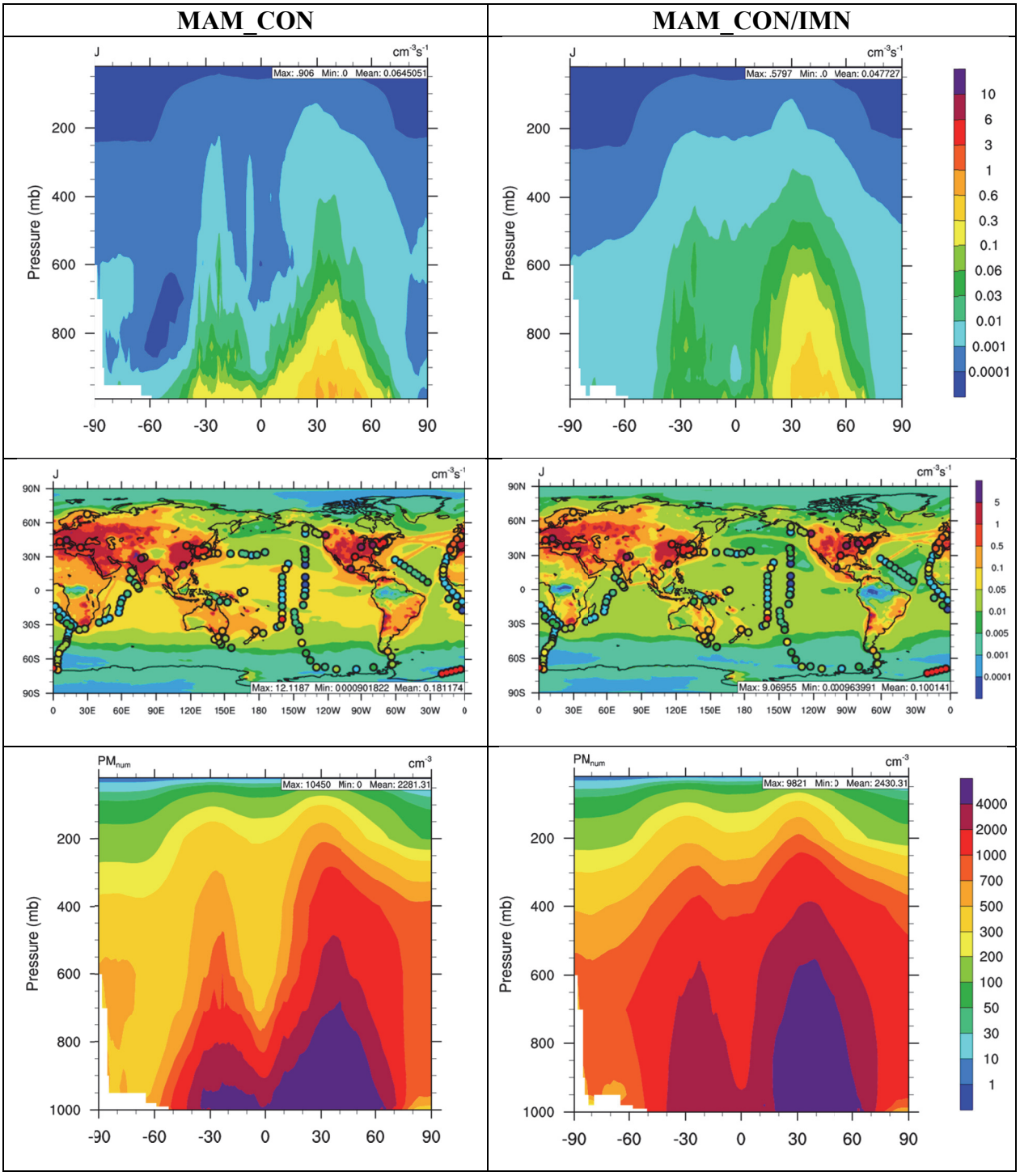

Figure 4. Vertical distribution of new particle formation rate (J) and aerosol number (PM_{num}) simulated by MAM_CON/IMN for 2001. The overlay plots show the distribution of J in bottom 1000-m. Circles on overlay plots represent observations for J. Different colors of circles represent different values of J, using the same color scale as simulated J.

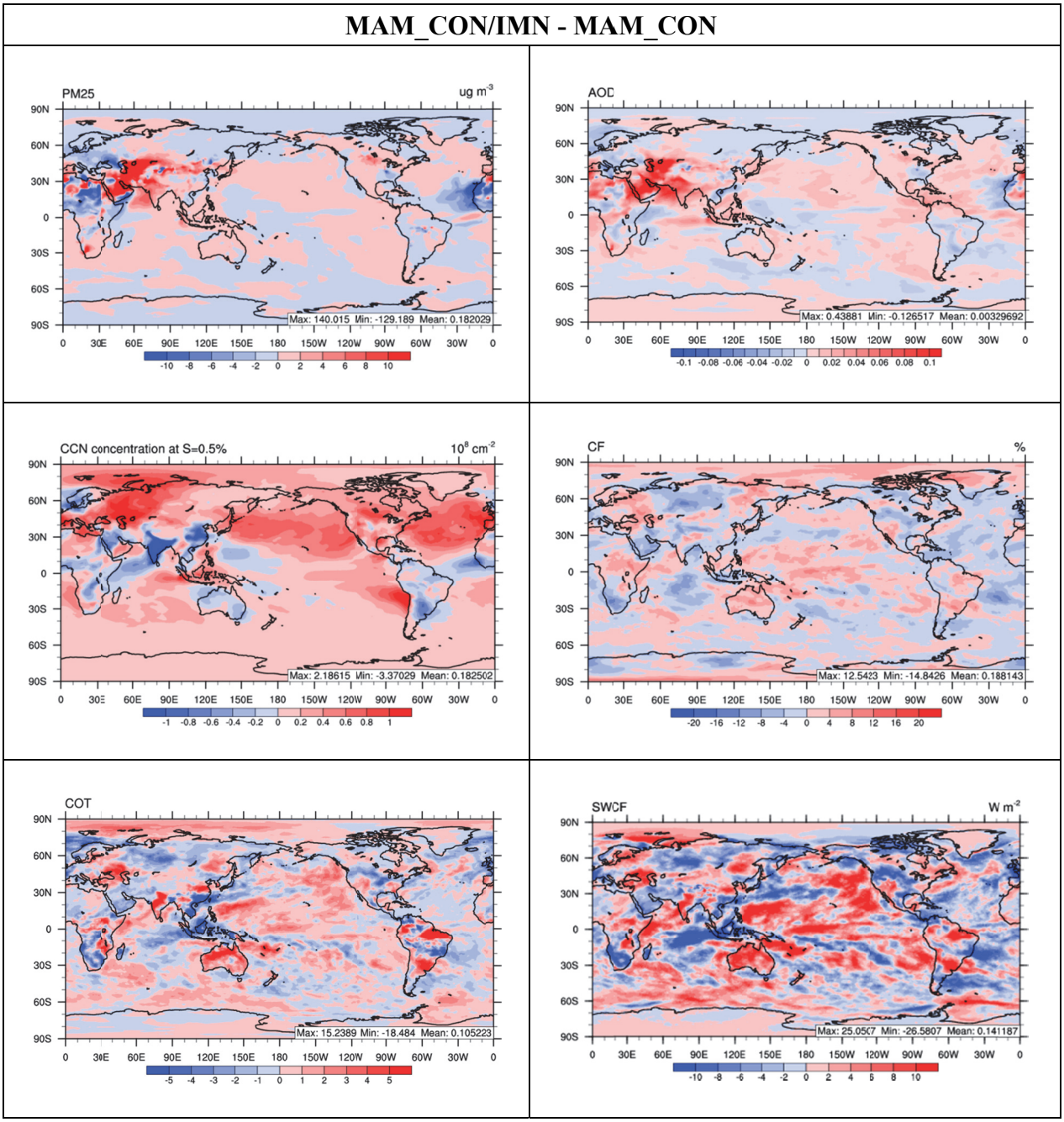

Figure 5. Absolute differences of $PM_{2.5}$, AOD, column CCN5, CF, COT, and SWCF between MAM_CON/IMN and MAM_CON for 2001.

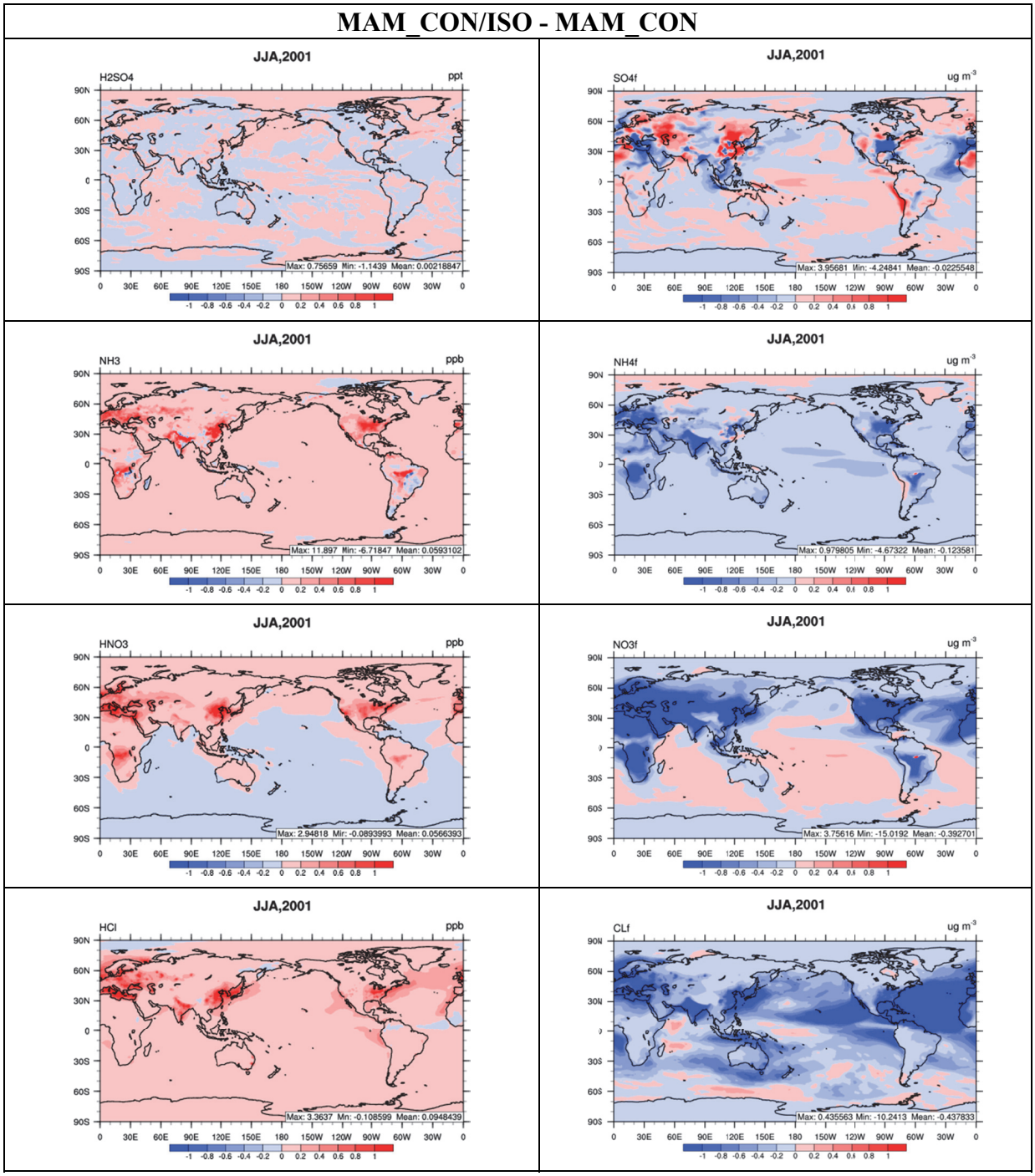

Figure 6. Absolute differences of major PM species and their gas precursors between MAM_CON/ISO and MAM_CON for summer, 2001.

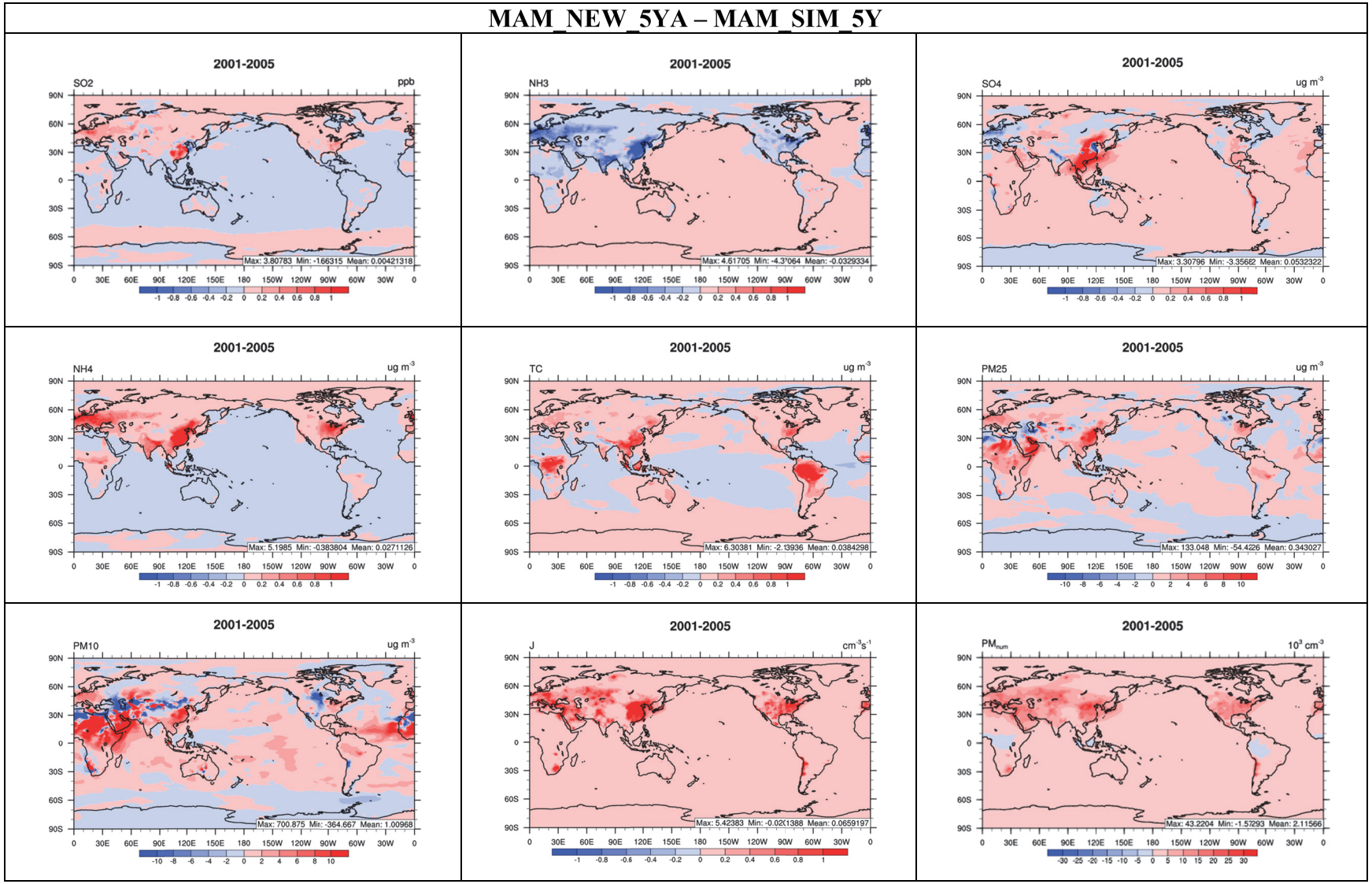

Figure 7. Absolute differences of major aerosol species and their gas precursors, new particle formation rate, and aerosol number between MAM_NEW_5YA and MAM_SIM_5Y for 2001-2005.

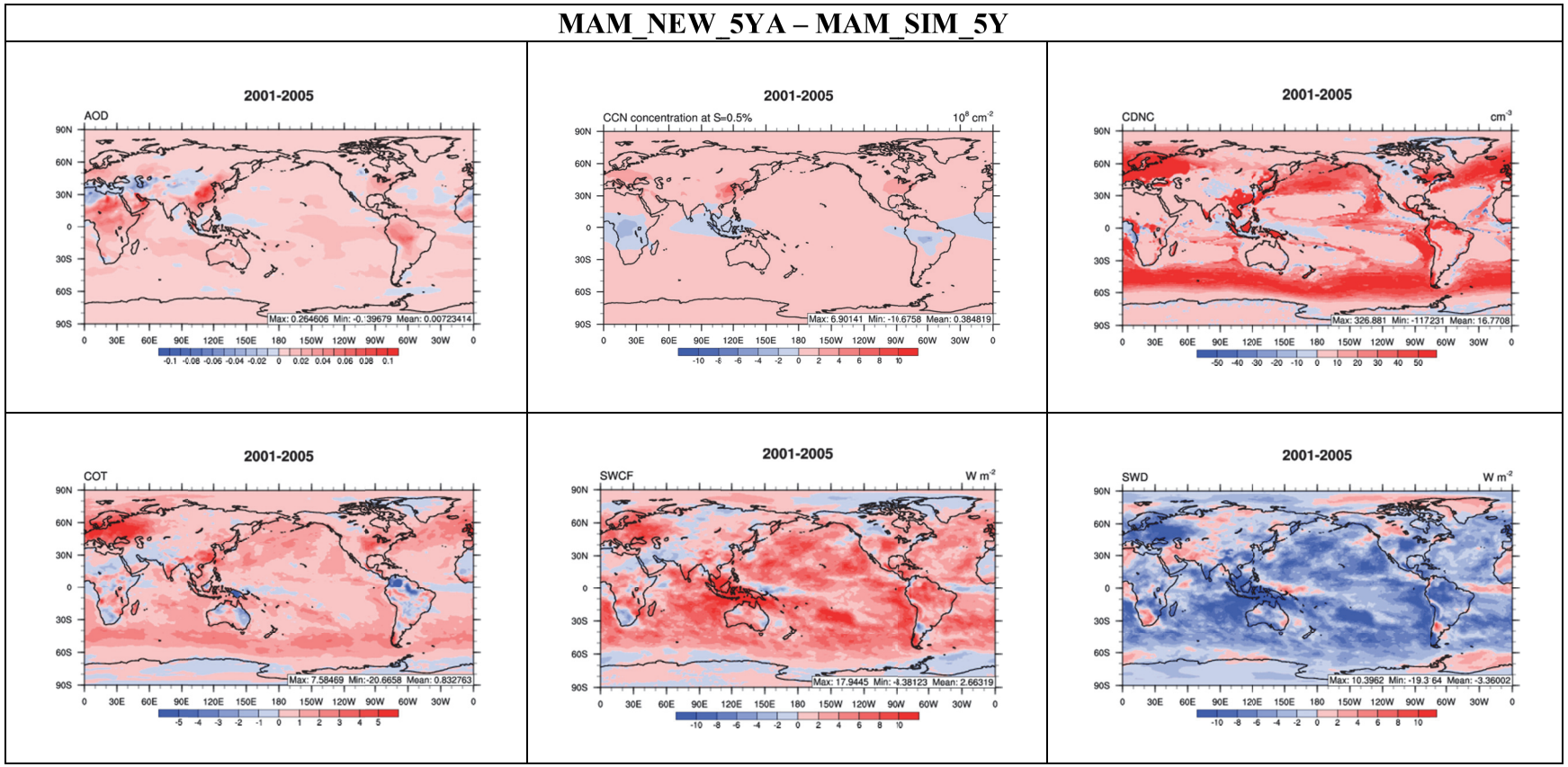

Figure 8. Absolute differences of major cloud and radiative variables between MAM_NEW_5YA and MAM_SIM_5Y for 2001-2005.